Numerical study on dynamical behavior in oscillatory driven quantum double-well systems

Akira Igarashi*
Graduate School of Science and Technology, Niigata University, Ikarashi 2-Nochou 8050, Niigata 950-2181, Japan

Hiroaki Yamada
YPRL, 5-7-14 Aoyama, Niigata 950-2002, Japan

(Received 7 September 2007; revised manuscript received 7 May 2008; published 26 August 2008)

We numerically investigate quantum dynamics in a one-dimensional double-well system emphasizing influence of a parametrically polychromatic perturbation on the dynamics. It is found that time dependence of transition probability for an initially localized wave packet between the wells shows two types of motion, coherent and incoherent motion, depending on the perturbation parameters. As the strength and/or the number of frequency components of the perturbation increase, coherent motion changes into incoherent one. The former is related to coherent tunneling of the wave packet due to coherence; the latter is related to a delocalized state caused by decoherence. In coherent motion, by virtue of coherence of the dynamics, the expectation value and the standard deviation of a dynamical variable such as the energy of the system show oscillatory time dependence around the initial values. On the contrary in incoherent motion, because of the decoherence, the time dependence fluctuates irregularly around a certain value after a rapid increase due to the resonance. We find that negativity of the Wigner function also show similar time dependence in each type of motion. We compare the classification of the quantum dynamics based on regularity of the time dependence with the one of corresponding classical dynamics based on the Lyapunov exponent. The classifications of the quantum and classical dynamics overlap well in the parameter space. Furthermore, we confirm decoherence of quantum dynamics in a kicked double-well system.

DOI: 10.1103/PhysRevE.78.026213 PACS number(s): 05.45.Mt, 03.65.−w

I. INTRODUCTION

Quantum dynamics in classically chaotic systems has attracted much attention during several decades. In particular it has been of great interest to investigate influence of classical chaos on quantum-mechanical phenomena related to quantum coherence, such as tunneling, dynamical localization of a wave packet, and decoherence.

Recent studies have revealed that classical chaos affects quantum tunneling drastically. When classical dynamics shows chaos, the corresponding quantum system exhibits remarkable enhancement of coherent tunneling, so-called chaos assisted tunneling [1–4]. The chaos assisted tunneling is triggered by an intermediate state which resides in a chaotic region of the corresponding classical phase space. Moreover influence of weak chaos on quantum tunneling is investigated in terms of nonlinear resonance [5,6]. In the connection with the present paper, we here refer to two famous quantum tunneling phenomena in a time-dependent one-dimensional double-well potential. Lin and Ballentine studied wave packet tunneling in a Duffing system without dissipation which shows strong chaotic dynamics in the classical limit [1]. They found that coherent tunneling occurs between symmetry-related Kolmogorov-Arnold-Moser tori which emerge in the phase space owing to strong nonlinear resonance. Because of the classical chaos, the tunneling frequency is enhanced by several order of magnitude compared to the unperturbed one. Chaos assisted tunneling is experimentally observed recently in various systems, for instance, a cold cesium atom in an amplitude-modulated standing wave of light [7]; transfer of light power between the two optical waveguides [8]. On the other hand, the second example is quite opposite to the first one. Grossmann *et al.* studied coherent destruction of tunneling in a Duffing system as well as Lin *et al.* did but with different perturbation parameters [9]. They found a one-dimensional manifold in the parameter space spanned by the amplitude and the frequency of the perturbation where the tunneling between the wells is completely suppressed. This suppression is attributed to the fact that the time scale of the tunneling diverges because the two states of the ground state doublet, which is responsible for the tunneling, intersect each other on the manifold. The suppression of tunneling is also experimentally observed in an optical double-well system [10].

On the other hand, localization of a wave packet in a classically chaotic system has also been studied from the point of view of quantum coherence [11–15]. For instance, in a kicked rotor system, quantum dynamics mimics the corresponding classical dynamics for only a short time scale which is proportional to the squared value of the kicking strength divided by that of Planck constant. After the time scale, the wave function starts to localize because of the quantum coherence, whereas the corresponding classical dynamics continues to diffuse in the momentum space. The destruction of the localization in the kicked rotor system has been investigated by applying another external field in Ref. [11] or by introducing a noise to the system in Ref. [15]. Especially noise-induced delocalization in the kicked system is experimentally confirmed recently for cesium atoms in a modulated one-dimensional optical lattice [16]. Effect of a classical accelerator mode on the delocalization of a wave

*igara4.akira@gs.niigata-u.ac.jp

packet and the momentum diffusion is also discussed in Ref. [17].

Moreover, it is well known that a quantum system loses coherence when it is coupled to another system which consists of many degrees of freedom, i.e., *environment* [18]. The coupling to the environment changes the quantum system into the classical system because of decoherence [19]. For instance, Habib *et al.* showed that decoherence brings a smooth quantum-to-classical transition in a classically chaotic system which is coupled to environment [20]. It has also reported that chaotic degrees of freedom which are coupled to a quantum system of interest plays an equivalent role to decoherence of the system [21].

As far as the present authors know, it is less well known that how parametric instability affect the quantum dynamics in a one-dimensional time-dependent double-well system, in spite of the classical significance [22,23], whereas the effect of instability induced by forced oscillation on the dynamics is well investigated. (See, for instance, Ref. [24].) Therefore we consider quantum dynamics as well as classical dynamics in a parametrically driven one-dimensional double-well system. In a previous paper [25], we have investigated quantum dynamics in a one-dimensional double-well system which is parametrically driven by a monochromatic external field. It has been found that quantum tunneling between the wells is broken by the perturbation with relatively large perturbation strength when the driving frequency is close to resonance, while the quantum tunneling is enhanced when the frequency is off-resonant to the intrinsic frequency in the unperturbed system.

In the following, we use the term *decoherence* in the sense of irregularity of quantum dynamics which brings delocalization phenomena of a wave packet. Contrary to this, regular dynamics has coherence, i.e., constructive interference, which gives localization property to a wave function. In other words, decoherence causes the destruction of the constructive interference as observed for some perturbed cases by external noise. Indeed, once decoherence occurs, a wave packet cannot localize again within a realistic time scale after the delocalization caused by the perturbation in the system we here deal with.

We investigate how the polychromatic perturbation influences the dynamics, on the basis of numerical results of quantum and classical dynamics in a parametrically driven one-dimensional double-well system. We find that the qualitative change of the wave packet dynamics occurs as the strength and/or the number of frequency components of the perturbation increase. The polychromatic perturbation can enhance coherent tunneling between the wells as the perturbation strength increases. On the other hand, the perturbation can also induce decoherence of the quantum dynamics when the perturbation strength increases further. This implies existence of a critical perturbation strength depending on the number of frequency components. Exceeding the critical perturbation strength changes the coherent quantum motion to an incoherent one which is related to a delocalized wave function due to destruction of coherence.

In Ref. [26], we have reported some preliminary results concerning the enhancement of the tunneling and decoherence in the polychromatically perturbed double-well system. In the present paper, we give the extended results as well as aspects by the Wigner function. Comparing with the previous paper, the present one has the following characteristics: (i) The quantum dynamics is considered in detail through the time evolution of the wave function and the validity of the two-level approximation. (ii) Comparison between the classical-quantum dynamics is directly shown. (iii) The universality of the phenomenon is discussed by giving numerical results for another system, the kicked double-well system. (iv) The quantum dynamics under a stochastic perturbation is dealt with in more detail than the previous one. (v) Numerical results on the resonance of transition probability and fidelity are also given.

The organization of this paper is as follows. In Sec. II we introduce the model and the basic feature. In particular, we emphasize the essential difference between our model and a familiar one which is used in many other works.

In Sec. III we classify the classical dynamics with particular emphasis on the perturbation parameter dependence of the numerically obtained Lyapunov exponent.

In Sec. IV we show numerical results on the transition probability between the potential wells for an initially localized wave packet. We introduce a quantity which measures regularity of time dependence of the transition probability. We classify type of quantum motion on the basis of the parameter dependence of the quantity. Through this classification, we show that the qualitative change occurs in the quantum dynamics.

In Secs. V and VI, we give properties of the wave packet dynamics in detail for each case which is classified in Sec. IV, focusing on time dependence of the expectation value and the standard deviation of the energy, the uncertainty product, and the Hushimi representation of a wave function. There is quantitative change in the time dependence of such quantities from oscillation to irregular fluctuation. We discuss the types of the corresponding quantum dynamics on the basis of validity of a two-level approximation and influence of the underlying classical chaos.

In Sec. VII, we discuss quantum-classical correspondence comparing the time evolution of the Wigner function with that of classical phase space density. Moreover, we give numerical results of negativity of the Wigner function in order to make the difference between coherent and incoherent motion clear.

In Sec. VIII, we show coherent tunneling and decoherence in a kicked double-well system. We confirm that kicking impulse brings not only enhancement of coherent tunneling but also decoherence of the quantum dynamics as well as the polychromatic perturbation does.

Section IX is devoted to the summary of the present paper.

In Appendix A, we give a brief comment on resonance in time dependence of the transition probability. In Appendix B, we show numerical results on wave packet dynamics under a stochastic perturbation, in order to compare with that under the polychromatic perturbation. Then we also briefly refer to the relationship of our treatment of the stochastic perturbation and the stochastic Schrödinger equation. In Appendix C we give numerical results on fidelity in the system which is commonly used as a measure of coherence of quantum dynamics.

II. MODEL

We consider dynamics in a driven one-dimensional double-well system which has the following Hamiltonian:

$$H(p,q,t) = \frac{p^2}{2} + V(q,t), \tag{1}$$

$$V(q,t) = V_0(q) + V_1(q,t), \tag{2}$$

$$V_0(q) = \frac{q^4}{4} - \frac{a}{2}q^2. \tag{3}$$

Here p and q represent the canonically conjugate momentum and coordinate, respectively. We set Planck constant $\hbar=1$ for quantum-mechanical calculation throughout the present paper. The potential $V(q,t)$ consists of two parts; $V_0(q)$ represents the unperturbed double-well potential and $V_1(q,t)$ the time-dependent perturbation. The parameter a in $V_0(q)$ adjusts the depths of and the distance between the wells. We take $a=5$ throughout the present paper. Then the frequency $\omega_{\rm cl}^0$ of the classical harmonic oscillator around an unperturbed potential well is given by $\omega_{\rm cl}^0=\sqrt{2a}=\sqrt{10}\simeq 3.16$. The time-dependent perturbation takes the form

$$V_1(q,t) = \frac{A(t)}{2}q^2, \tag{4}$$

where

$$A(t) = \frac{1}{\sqrt{M}}\sum_{i=1}^{M} \epsilon_i \sin(\Omega_i t + \theta_{i0}) \tag{5}$$

is the external field which parametrically drives the unperturbed system. The external field $A(t)$ consists of M sinusoidal modes which are coupled to the system with strength ϵ_i. For the sake of simplicity, we set $\epsilon_i=\epsilon$ for all i and $\epsilon=0.1, 0.2, \ldots, 1.0$. Then under the setting $\hbar=1$, the perturbed quantum system has several energy doublet for each value of ϵ. The frequency of ith sinusoidal mode in $A(t)$ is represented by Ω_i. We set the frequencies Ω_i's of the perturbation as mutually incommensurate. The incommensurate relationship breaks the periodic time dependence of the Hamiltonian and disables it from an approach based on the Floquet theory. Moreover, we take Ω_i's to be around unity. Then Ω_i's are off resonant in the unperturbed system both classical and quantum mechanically,

$$\Omega_i \ncong \omega_{\rm cl}^0 \quad \text{and} \quad \Omega_i \ncong \Delta E_{02}^0 \quad (i=1,2,\cdots,M), \tag{6}$$

where ΔE_{02}^0 is the energy difference between the ground state doublet and the first excited one in the unperturbed system (see Table I). The initial phases of the modes of $A(t)$ is represented by θ_{i0} which are uniform random number in the range $[0, 2\pi]$. For a different combination of the frequencies $\{\Omega_i\}$ and the initial phases $\{\theta_{i0}\}$, we confirmed that the following results in the present paper are almost similar if Ω_i's are off resonant. We refer to quantum dynamics under the perturbation with resonant frequencies in Appendix A.

TABLE I. Eigenenergy and energy difference in the unperturbed system. Here n denotes the quantum number, E_n^0 eigenenergy, ΔE_{nm}^0 the energy difference between the nth and mth eigenenergy in the unperturbed system.

n	E_n^0	$\Delta E_{n,n-1}^0$
0	−4.723	
1	−4.722	6.747×10^{-4}
2	−1.960	2.762
3	−1.910	5.033×10^{-2}
4	-6.723×10^{-3}	1.954
5	6.349×10^{-1}	6.416×10^{-1}
6	2.018	

Snapshots of the potential and some lowest energy levels of the unperturbed system are illustrated in Fig. 1. Several eigenvalues and energy differences between them of the unperturbed system are given in Table I.

During the time evolution, the system remains symmetric with respect to reflection of q, $H(p,-q,t)=H(p,q,t)$, and the energy of the separatrix is always zero in this model. These two properties give some essential difference from other works using a Duffing-type system. Note that we use the term a "Duffing-type system" in the sense of a dissipationless double-well system whose unperturbed potential is given by $V_0(q)$, which is similar to our system but whose time-dependent perturbation is proportional to q $[V_1(q,t)\propto q]$ unlike our system. First, whenever there exists an eigenstate of the Hamiltonian with a negative eigenvalue, the symmetry always gives the ground state doublet. This doublet is responsible for wave packet tunneling when the wave packet fully populates in the doublet. Secondly, an adiabatic transition between instantaneous eigenstates is concerned. The instantaneous eigenstates are obtained by $H(t)|n(t)\rangle = E_n(t)|n(t)\rangle$. Then the time-dependent Schrödinger equation can be expressed in the following form:

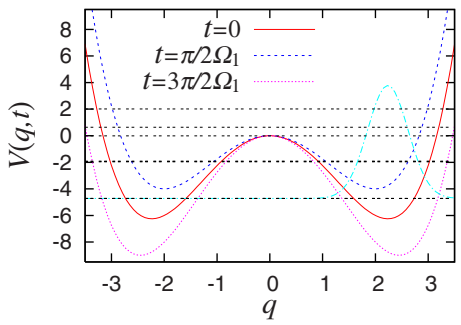

FIG. 1. (Color online) Snapshots of the driven double-well potential, energy eigenvalues, and the initial wave packet [Eq. (9)]. The potential curves are described for the case $M=1$ with $\epsilon=1.0$ at $t=0, \pi/2\Omega_1$, and $3\pi/2\Omega_1$. The horizontal lines represent the seven lowest energy eigenvalues of the unperturbed system. There are two doublets under the top of the potential barrier. The initial packet is enlarged by 10 times in the vertical direction.

$$\frac{da_n(t)}{dt} = -ia_n(t)E_n(t) + \sum_{m(\neq n)=0}^{\infty} a_m(t)\frac{\langle n(t)|\partial H(t)/\partial t|m(t)\rangle}{E_n(t) - E_m(t)}, \tag{7}$$

where $a_n(t)$'s are the expanding coefficients of the wave function, i.e., $|\psi(t)\rangle = \Sigma_{n=0}^{\infty} a_n(t)|n(t)\rangle$. The second term of the right-hand side in Eq. (7) represents an adiabatic transition between instantaneous eigenstates of $H(t)$. Because $\partial H(t)/\partial t \propto q^2$ and each eigenstate $|n(t)\rangle$ is an even or odd function of q, an adiabatic transition occurs between the same parity only, unlike a Duffing-type system [27]. Note that, when such a system is perturbed polychromatically, an instantaneous eigenstate has no parity symmetry even including generalized parity. This indicates that the transition amplitude described by $\langle n(t)|\partial H(t)/\partial t|m(t)\rangle$ in the second term of Eq. (7) survives for substantially all m in a Duffing-type system. Therefore an adiabatic transition occurs less frequently in our system than a Duffing-type one. Moreover when the driving $A(t)/2$ is replaced by a noise in the corresponding classical Newton equation of motion, the noise is included as a *multiplicative* noise in our system [see Eq. (8)], not as an additive one.

III. CORRESPONDING CLASSICAL DYNAMICS

Before showing numerical results on the quantum dynamics, we consider the corresponding classical dynamics focusing especially on perturbation parameter dependence of the maximum Lyapunov exponent. The equation of motion of the classical dynamics is given as

$$\frac{d^2q}{dt^2} = -[q^3 + A(t)q]. \tag{8}$$

The time-dependent perturbation is included parametrically.

Figure 2 shows the classical phase space structure for some combinations of the perturbation parameters, i.e., the perturbation strength ϵ and the number M of the frequency components of the perturbation. In order to obtain clear quantum-classical correspondence, we set the initial points uniformly around the center of the right well according to the initial wave packet of Eq. (9) in the quantum dynamics.

In Figs. 2(a) and 2(b), the classical trajectories are fully confined in the initially prepared potential well with a regular structure and do not extend over the wells. When $M=1$ with $\epsilon=0.1$ shown in Fig. 2(a), the trajectories form Kolmogorov-Arnold-Moser tori. On the contrary, when $M=2$ with $\epsilon=0.1$ shown in Fig. 2(b), the trajectories have the width originating from the polychromatic time dependence of the Hamiltonian. The width of a trajectory grows with the increase of M and/or ϵ. The regular structure mentioned above dominates the phase space structure even for a relatively large perturbation strength because of the off-resonant frequencies of the perturbation. In these cases a chaotic region in the phase space is restricted only around the unperturbed separatrix.

We see global chaotic behavior in Figs. 2(c) and 2(d). As M and/or ϵ increase further, the regular structures are gradually destroyed and replaced by a global chaotic sea because of the overlapping resonance [28,29]. In the case shown in

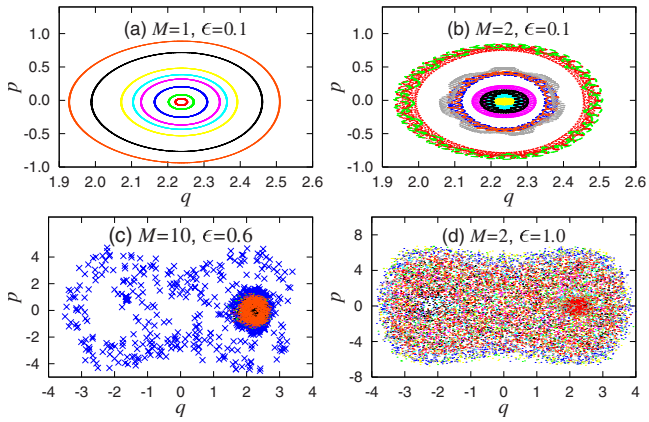

FIG. 2. (Color online) Classical phase space structures for some combinations of the perturbation parameters ϵ and M. The initial points are distributed uniformly around the center of the right well for the sake of quantum-classical correspondence. The combinations of the perturbation parameters are (a) $M=1$, $\epsilon=0.1$; (b) $M=2$, $\epsilon=0.1$; (c) $M=10$, $\epsilon=0.6$; (d) $M=10$, $\epsilon=1.0$. Stroboscopic plots are taken at times $t=2\pi n/\Omega_1$ $(n=0,1,2,\ldots)$. Note that the plots are not exact Poincaré surface of the section because of the polychromatic time dependence of the Hamiltonian. In panel (c) a global chaotic trajectory is denoted by a large point (cross).

Fig. 2(c), some trajectories escape from the right well which seem to be chaotic, while most of the trajectories still localize in the right well against the perturbation. In Fig. 2(d), we find that almost all trajectories show global chaotic behavior not being confined in the right well.

In order to numerically estimate the stability of a trajectory, we calculate the maximum Lyapunov exponent $\lambda_{\mathrm{cl}}^{\max}$ within *finite time interval* $t \in [0,T]$, where the definition of T is given in Sec. IV. We give the perturbation parameter dependence of $\lambda_{\mathrm{cl}}^{\max}$ in Fig. 3. From Fig. 3(a) we see strong chaotic motion occurs when $M \geqslant 3$ in the present system. We also see that $\lambda_{\mathrm{cl}}^{\max}$ increases rapidly as the perturbation strength increases once the trajectory becomes chaotic.

Figure 4 represents the roughly estimated phase diagram of $\lambda_{\mathrm{cl}}^{\max}$ in the parameter space spanned by M and ϵ. In this phase diagram we classify degree of chaos of the classical dynamics depending on the value of $\lambda_{\mathrm{cl}}^{\max}$ in the following way: (i) When $0 < \lambda_{\mathrm{cl}}^{\max} < 0.04$, almost all trajectories are confined in the initially prepared well with regular motion. (ii) When $0.08 < \lambda_{\mathrm{cl}}^{\max}$, almost all trajectories show global chaotic motion. (iii) When $0.04 < \lambda_{\mathrm{cl}}^{\max} < 0.08$, the motion is weakly chaotic, i.e., neither globally chaotic nor fully regular. This corresponds to the intermediate motion between the regular and the globally chaotic motion. We see two types of typical motion, i.e., regular and chaotic motion, are divided by weak chaotic motion. We refer to the region of the phase diagram in which the classical motion is regular (chaotic) as *the regular (chaotic) motion regime* in the present paper. We see a similar structure of the phase diagram for quantum dynamics in the next section.

From the classical dynamics shown above, we may naively expect that the quantum tunneling is enhanced by the classical chaos as seen in the chaos assisted tunneling mentioned in the Introduction [1–4]. In the next section we see that this is not always true.

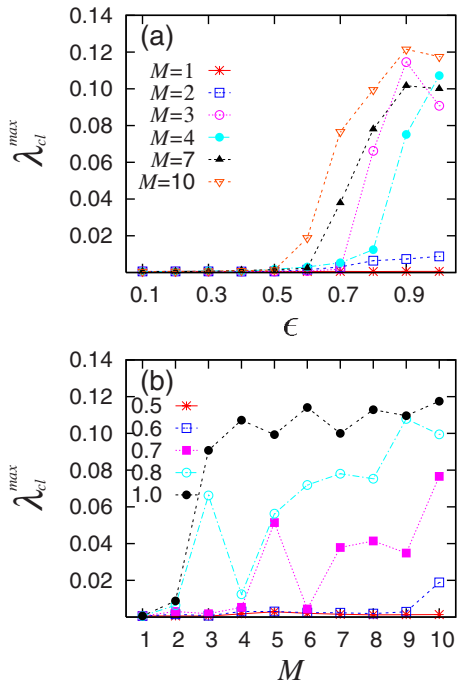

FIG. 3. (Color online) Perturbation parameter dependence of the maximum Lyapunov exponent $\lambda_{\mathrm{cl}}^{\max}$. The upper panel (a) describes the ϵ dependence for various M's; the lower panel (b) the M dependence for various ϵ's.

IV. TRANSITION PROBABILITY AND DEGREE OF COHERENCE

In this section we show numerical results on wave packet dynamics in the system. On the basis of time dependence of transition probability between the potential wells, we classify quantum-dynamical behavior.

A. Initial state and numerical setting

In order to trace the wave packet dynamics in the system, we use the following Gaussian wave packet as the initial state which is localized in the right well of the potential,

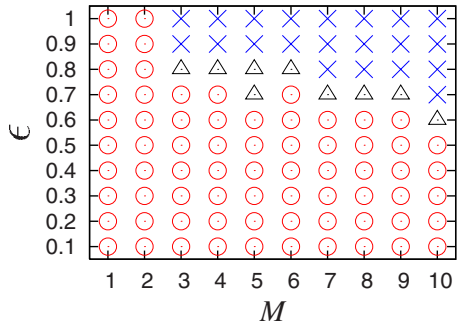

FIG. 4. (Color online) Phase diagram of Lyapunov exponent. Circle (○) denotes regular motion ($0.0<\lambda_{\mathrm{cl}}^{\max}<0.04$); triangle (△) weak chaotic one ($0.04<\lambda_{\mathrm{cl}}^{\max}<0.08$); cross (×) strong chaotic one ($0.08<\lambda_{\mathrm{cl}}^{\max}$).

$$\psi(q,t=0)=(\sigma\pi)^{1/4}\exp\left[-\frac{(q-q_0)^2}{2\sigma}\right], \tag{9}$$

where $q_0=\sqrt{a}\simeq 2.236$ is the right bottom of the unperturbed potential well and $\sigma=1/3.4\cong 0.3$ is the initial spread of the wave packet. This wave packet describes accurately an equal-weight linear combination of the ground state doublet in the unperturbed system,

$$|\psi(t=0)\rangle\cong\frac{1}{\sqrt{2}}[|0(t=0)\rangle+|1(t=0)\rangle], \tag{10}$$

with an appropriate choice of the relative phase. In the unperturbed system, this wave packet shows coherent tunneling between the wells because of interference between the two states of the ground state doublet [30]. The recurrence time T of this tunneling is given by $T\equiv 2\pi\hbar/\Delta E_{01}^{0}\cong 9.4\times 10^{3}$, where ΔE_{01}^{0} is the energy split in the ground state doublet in the unperturbed system as given in Table I. Therefore, the time scale T can be used for a reference time when we consider influence of the polychromatic perturbation described by Eqs. (4) and (5) on the wave packet dynamics. We hence consider the wave packet dynamics in the time interval $t\in[0,T]$ in the following.

For numerical integration of the time-dependent Schrödinger equation, we use the second-order symplectic integrator [31],

$$|\psi(t+\Delta t)\rangle=\exp\left(-\frac{i}{\hbar}\frac{K\Delta t}{2}\right)\exp\left(-\frac{i}{\hbar}[V(q,t+\Delta t/2)]\Delta t\right)\times\exp\left(-\frac{i}{\hbar}\frac{K\Delta t}{2}\right)|\psi(t)\rangle+O(\Delta t^3), \tag{11}$$

where $K=p^2/2$ is the kinetic energy operator. We set the time mesh $\Delta t=2\pi/500\simeq 1.26\times 10^{-2}$, and the spatial one $\Delta q\simeq 4.72\times 10^{-2}$.

Under setting $\hbar=1$, *effective Planck constant* $\hbar_{\mathrm{eff}}\equiv\hbar/S_{\mathrm{char}}$ is estimated as $\hbar_{\mathrm{eff}}\sim 1/40$, where S_{char} is a characteristic value of a classical action that is the area enclosed by the unperturbed classical separatrix. Therefore, all the following consideration is in a purely quantum-mechanical realm.

B. Transition probability

We define *transition probability* $P_{\mathrm{L}}(t)$ which gives the probability that the wave packet is found in the left half side $q<0$,

$$P_{\mathrm{L}}(t)\equiv\int_{-\infty}^{0}|\psi(q,t)|^2dq, \tag{12}$$

where $\psi(q,t)$ represents the solution of the time-dependent Schrödinger equation with the initial condition of Eq. (9). When the perturbation strength is relatively small, the quantity $P_{\mathrm{L}}(t)$ can be interpreted as *tunneling* probability; the initially localized wave packet passes through the central energy barrier and reaches the left well by tunneling.

Figures 5 and 6 show time dependence of $P_{\mathrm{L}}(t)$ for various combinations of the perturbation parameters, i.e., the

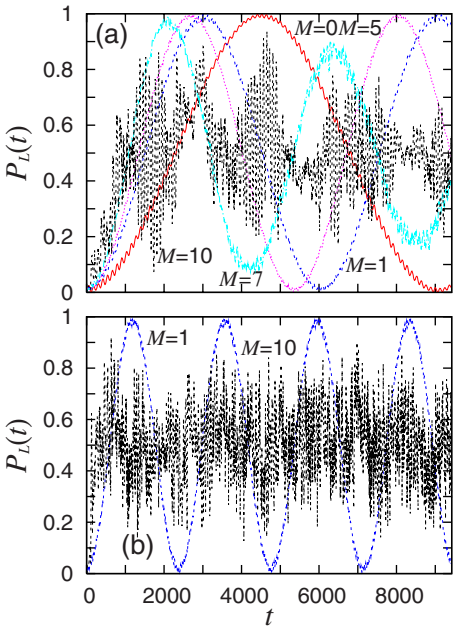

FIG. 5. (Color online) Perturbation strength dependence of transition probability $P_{\mathrm{L}}(t)$ as a function of time t for various M's. The values of ϵ are (a) $\epsilon=0.4$; (b) $\epsilon=0.8$. The curve with "$M=0$" in the upper panel (a) represents $P_{\mathrm{L}}(t)$ for the unperturbed case. The calculation time is almost same as the recurrence time of $P_{\mathrm{L}}(t)$ in the unperturbed case.

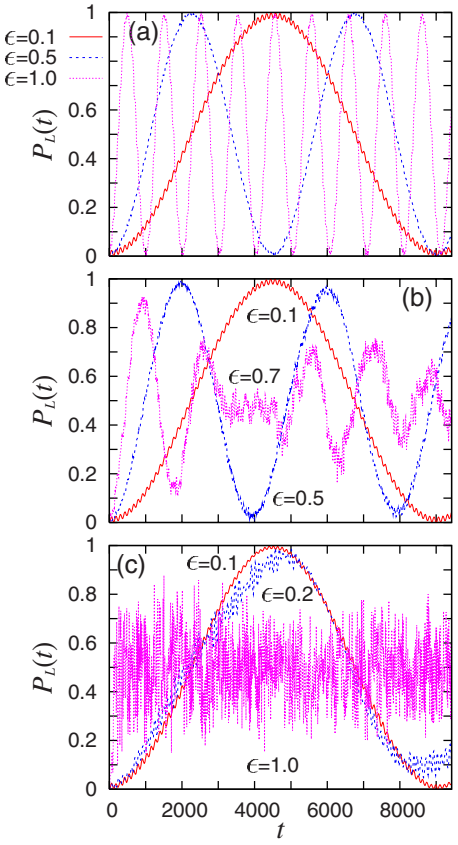

FIG. 6. (Color online) The number of frequency components dependence of $P_{\mathrm{L}}(t)$ as a function of time t for various ϵ's. The values of M are (a) $M=2$ with $\epsilon=0.1$, 0.5, and 1.0; (b) $M=5$ with $\epsilon=0.1$, 0.5, and 0.7; (c) $M=10$ with $\epsilon=0.1$, 0.2, and 1.0.

strength ϵ and the number M of the frequency component of the perturbation.

The curve labeled by "$M=0$" in Fig. 5(a) represents the time dependence of the tunneling probability in the unperturbed case. In the case, the coherent tunneling occurs which is mentioned in Sec. IV A and show regular oscillation with time t. We also find similar regular oscillations of $P_{\mathrm{L}}(t)$ with enhanced frequency when $M=1$ and $M=5$. The regularity suggests that quantum dynamics still has coherence and hence that $P_{\mathrm{L}}(t)$ still represents tunneling probability between the potential wells. In the present paper, we call this kind of motion *coherent motion*, whose definition is given in Sec. IV C. We observe small amplitude oscillation around the dominant oscillation of $P_{\mathrm{L}}(t)$ representing the tunneling in coherent motion. The small amplitude oscillation originates from higher excited states involved in the initial wave packet of Eq. (9). In coherent motion, the frequency of $P_{\mathrm{L}}(t)$ becomes larger as M increases. On the contrary, we see different types of time dependence of $P_{\mathrm{L}}(t)$, i.e., irregular fluctuation when $M=10$, and intermediate oscillation which is neither coherent nor irregular when $M=7$. In any cases shown above, in relatively short time scale $t\lesssim 1000$, we find enhancement of $P_{\mathrm{L}}(t)$ by the perturbation Eq. (4) compared to the unperturbed case. The increase of M gives larger enhancement which may be attributed to the increase of stochasticity in the corresponding classical dynamics as seen in chaos assisted tunneling.

Figure 5(b) shows the time dependence of $P_{\mathrm{L}}(t)$ for relatively large perturbation strength $\epsilon=0.8$. When $M=1$, we still find coherent oscillation of $P_{\mathrm{L}}(t)$ with the enhanced frequency due to the strong perturbation strength compared to the previous case $\epsilon=0.4$. On the other hand, when $M=10$, $P_{\mathrm{L}}(t)$ fluctuates irregularly compared to the case $\epsilon=0.4$.

Next we give the ϵ dependence of $P_{\mathrm{L}}(t)$ for various M's in Fig. 6. When $M=2$ shown in Fig. 6(a), $P_{\mathrm{L}}(t)$'s show coherent motion even for a large perturbation strength. It is clearly shown that the frequency of coherent motion becomes large as the perturbation strength increases. When $M=5$, shown in Fig. 6(b), a significant change does not occur for small perturbation strength ($\epsilon=0.1$), compared to the case $M=2$ with the same perturbation strength. However, the perturbation distorts coherent motion for relatively large perturbation strength, $\epsilon\gtrsim 0.6$, although the time dependence is not fully irregular when $\epsilon=0.7$. When $M=10$, shown in Fig. 6(c), coherent oscillation is not seen even for relatively small ϵ; even when $\epsilon=0.2$, we see slight but clearly different time dependence from that with $\epsilon=0.1$.

The above numerical results show that the polychromatic perturbation brings not only the enhancement but also the breakdown of coherent tunneling, depending on the perturbation parameters. Coherent tunneling is replaced by irregular fluctuation after some enhancement. Once coherent motion is broken by the perturbation Eq. (4), with increase of ϵ and/or M, the transition probability rapidly fluctuates around $P_{\mathrm{L}}(t)\sim 0.5$ and the amplitude of $P_{\mathrm{L}}(t)$ becomes smaller. These facts suggest that the wave function cannot localize in *either* of the potential wells. In the present system, we do not

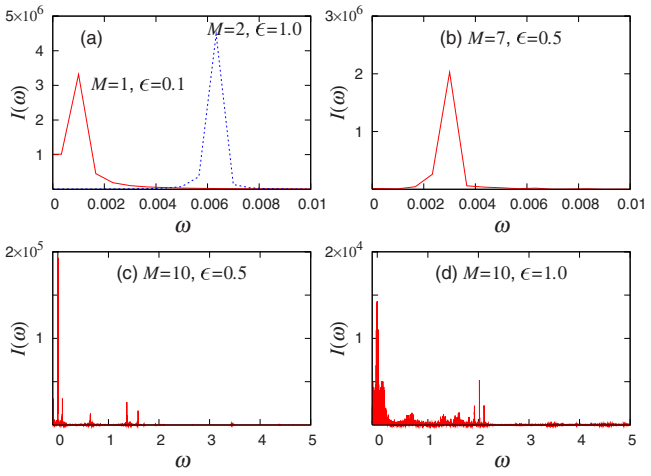

FIG. 7. (Color online) Fourier transform of transition probability for various combinations of the perturbation parameters. The combinations of the perturbation parameters are (a) $M=1$, $\epsilon=0.1$, and $M=2$, $\epsilon=1.0$; (b) $M=7$, $\epsilon=0.5$; (c) $M=10$, $\epsilon=0.5$; (d) $M=10$, $\epsilon=1.0$.

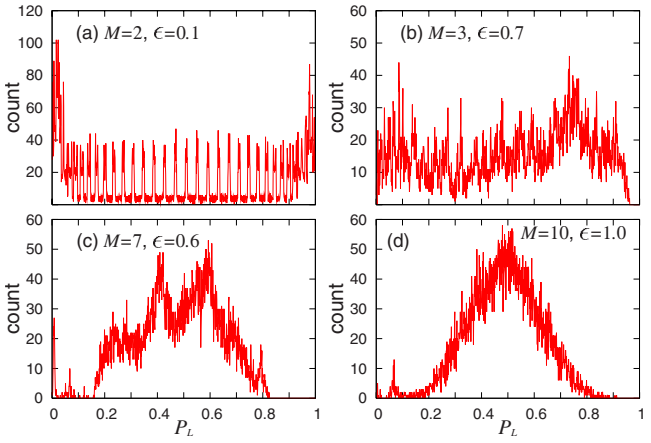

FIG. 8. (Color online) Histograms of transition probability for various combinations of the perturbation parameters. The vertical axes represent the number of the count that $P_{\mathrm{L}}(t)$ takes for a value in the segment $P_{\mathrm{L}}<P_{\mathrm{L}}(t)<P_{\mathrm{L}}+\delta P_{\mathrm{L}}$, where $0\leqslant P_{\mathrm{L}}<1$ with $|\delta P_{\mathrm{L}}|\ll 1$ during the time interval $[0,T]$. The combinations of the perturbation parameters are (a) $M=2$, $\epsilon=0.1$; (b) $M=3$, $\epsilon=0.7$; (c) $M=7$, $\epsilon=0.6$; (d) $M=10$, $\epsilon=1.0$.

observe a situation that a wave function settles down in *both* of the potential wells clearly splitting into the two parts, different from a situation discussed in Ref. [32]. If this situation would occur, the ground state doublet were still populated. However, when a wave function cannot localize, it is spread over the potential barrier, as we see in the following sections. This indicates that the ground state doublet is not occupied, and that, therefore, coherent tunneling breaks down.

We also observe that coherent motion breaks down for relatively small ϵ as M increases. We therefore expect that the quantum dynamics under a polychromatic perturbation approaches to that under a stochastic perturbation, as the number of frequency components of the polychromatic perturbation increases. Numerical results on quantum dynamics under a stochastic perturbation is given in Appendix B. On the other hand, when $P_{\mathrm{L}}(t)$ fluctuates irregularly, the time dependence is similar to that under a case driven by resonant frequencies which is given in Appendix A.

We next consider Fourier transform $I(\omega)$ of transition probability, in order to obtain a relevant time scale in $P_{\mathrm{L}}(t)$,

$$I(\omega)=\left|\int_0^T P_{\mathrm{L}}(t)\exp(-i\omega t)dt\right|^2. \tag{13}$$

Figure 7 gives ω dependence of $I(\omega)$ for several combinations of the perturbation parameters.

As shown in Figs. 7(a) and 7(b), there is only a single peak corresponding to the energy difference on the ω axis, if the ground state doublet effectively describes the dynamics on the basis of the two-level approximation. In this case we expect that the second term of the right-hand side of Eq. (7) is negligible. Then the wave function takes the form

$$|\psi(t)\rangle=\frac{1}{\sqrt{2}}[e^{-i\int_0^t E_0(s)ds}|0(t)\rangle+e^{-i\int_0^t E_1(s)ds}|1(t)\rangle]. \tag{14}$$

We have confirmed the validity of the two-level approximation in a monochromatic perturbation ($M=1$) in Ref. [26]. In this case, the oscillation period T_{osc} of $P_{\mathrm{L}}(t)$ is proportional to the averaged energy split in the ground state doublet with respect to the period of the time-dependent perturbation, i.e., $T_{\mathrm{osc}}\propto\frac{\Omega_1}{2\pi}\int_0^{2\pi/\Omega_1}[E_1(t)-E_0(t)]dt$. In other words, the averaged energy split in the ground state doublet is effectively enhanced by the perturbation. In Fig. 7(a), the effective enhancement is found for the case $M=2$ with $\epsilon=1.0$, compared to the one $M=1$ with $\epsilon=0.1$. We see that the enhancement appears in terms of the period of $P_{\mathrm{L}}(t)$ in Fig. 6(a). The enhancement of the energy split in the ground state doublet brings the enhanced frequency of coherent tunneling as discussed in Ref. [33].

When $M=7$ with $\epsilon=0.5$ shown in Fig. 7(b), in spite of the weak irregular time dependence of $P_{\mathrm{L}}(t)$, $I(\omega)$ does not show prominent difference from those shown in Fig. 7(a). On the other hand, when $M=10$ with $\epsilon=0.5$ shown in Fig. 7(c) in which $P_{\mathrm{L}}(t)$ fluctuates irregularly, we clearly see different ω dependence of $I(\omega)$. When $P_{\mathrm{L}}(t)$ fluctuates irregularly, the number of peaks of $I(\omega)$ increases. Moreover the width around a peak broadens with the increase of ϵ as shown in Fig. 7(d). As a result, from Fig. 7, we clearly see the breakdown of the two-level approximation as M and/or ϵ increase, which causes decoherence of the dynamics.

C. Degree of coherence

In order to make clear the difference between coherent motion, irregular fluctuation, and intermediate motion observed above, we deal with a histogram of transition probability. In Fig. 8, the histograms are shown by projecting the time dependence of $P_{\mathrm{L}}(t)$ onto the P_{L} axis for several combinations of the perturbation parameters.

In the case of coherent motion shown in Fig. 8(a), the two prominent peaks appear at the edges $P_{\mathrm{L}}=0$ and $P_{\mathrm{L}}=1$, as expected from the fact that the tunneling probability in the unperturbed system has sinusoidal time dependence [30].

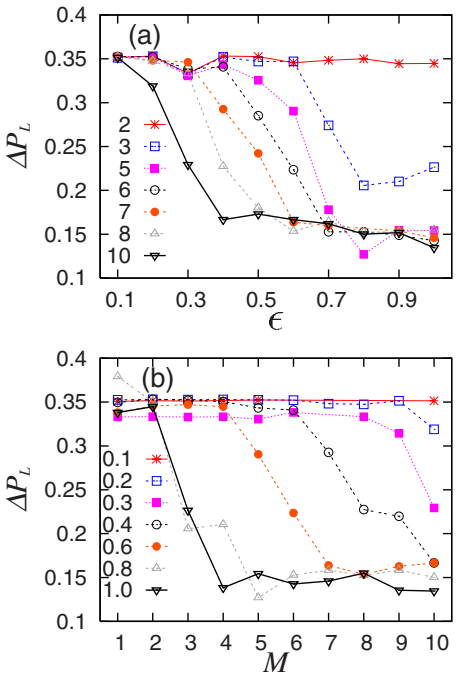

FIG. 9. (Color online) Perturbation parameter dependence of degree of coherence ΔP_{L}: (a) ϵ dependence for various M's, (b) M dependence for various ϵ's.

The existence of the two peaks at the edges indicates the occurrence of coherent motion because the wave packet can localize in either of the potential wells by tunneling. On the other hand, as shown in Fig. 8(b), the peaks become smaller owing to the increase of irregularity in the quantum dynamics as ϵ and/or M increase. In this case, the wave function cannot localize in either well. As quantum dynamics becomes irregular, the form of the corresponding histogram finally approaches to a bell-like shape as shown in Figs. 8(c) and 8(d). The behavior means that the motion of the wave packet cannot be associated with tunneling.

We next define *degree of coherence* ΔP_{L} based on the fluctuation of transition probability in order to obtain the quantitative difference between coherent motion, irregular fluctuation, and intermediate motion,

$$\Delta P_{\mathrm{L}} \equiv \{\overline{[P_{\mathrm{L}}(t) - \overline{P_{\mathrm{L}}}]^2}\}^{1/2}, \tag{15}$$

where $\overline{P_{\mathrm{L}}} \equiv \frac{1}{T}\int_0^T P_{\mathrm{L}}(t)dt$ represents the time average of $P_{\mathrm{L}}(t)$ over the time interval $[0,T]$.

Figure 9 shows perturbation parameter dependence of ΔP_{L}. From Fig. 9(a), when $M \leqslant 2$, ΔP_{L}'s maintain an almost constant value against the perturbation. On the contrary, when $M \geqslant 3$, we find that coherent motion breaks down where ΔP_{L}'s converge to a certain value after the decrease around a certain perturbation strength. Figure 9(b) gives the dependence of ΔP_{L} on the number M of frequency components. We confirm that irregular time dependence of $P_{\mathrm{L}}(t)$ appears even for a smaller perturbation strength as M increases.

On the basis of the value of ΔP_{L} for each combination of the perturbation parameters, we roughly divide the type of motion into three types as follows: (i) *Coherent motion*: In this case ΔP_{L}'s take almost similar value to the unperturbed one, i.e., $\Delta P_{\mathrm{L}} \gtrsim 0.3$. A wave packet can localize in either of the potential wells by coherent tunneling, because coherence of the dynamics fully survives. (ii) *Incoherent motion*: In this case the value of ΔP_{L}'s becomes much smaller than ones of coherent motion, i.e., $\Delta P_{\mathrm{L}} \lesssim 0.2$. The small value of ΔP_{L} represents that the wave function cannot localize in either well. The delocalized wave function is brought by decoherence of the dynamics. (iii) *Quasicoherent motion*: This corresponds to intermediate motion between the above ones. In this case the values of ΔP_{L}'s satisfy $0.2 \lesssim \Delta P_{\mathrm{L}} \lesssim 0.3$. We here emphasize that the existence of the qualitative change from coherent motion to the incoherent one is much more important than the exact value itself of ΔP_{L} which is needed to divide the type of motion into three types.

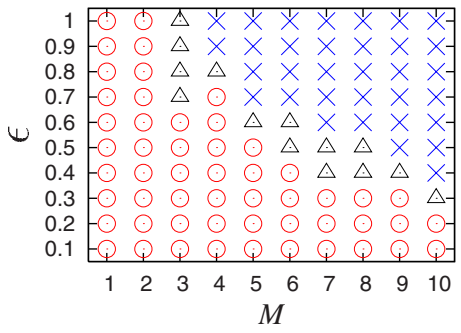

FIG. 10. (Color online) Phase diagram of the quantum motion based on the value of ΔP_{L}. Different marks represents different types of motion. Circle (○), triangle (△), and cross (×) indicate coherent ($\Delta P_{\mathrm{L}} > 0.3$), quasicoherent ($0.2 < \Delta P_{\mathrm{L}} < 0.3$), and incoherent motion ($\Delta P_{\mathrm{L}} < 0.2$), respectively.

Figure 10 represents the phase diagram of the quantum dynamics which states the classification of quantum motion, based on the value of ΔP_{L} in the parameter space. It seems that the two kinds of motion, i.e., coherent and incoherent motion, are divided by the thin layer corresponding to quasicoherent motion. We refer to the region in which coherent (incoherent) motion occurs as *the coherent (incoherent) motion regime* in this paper.

The above numerical estimation suggests the existence of the critical values $\epsilon_{\mathrm{c}}(M)$ of the perturbation strength depending on the number of the frequency component. When the perturbation strength exceeds the critical value $\epsilon_{\mathrm{c}}(M)$ for a fixed M, the quantum dynamics loses the coherence and becomes irregular.

We next consider quantum-classical correspondence through the relationship between the behavior of ΔP_{L} and $\lambda_{\mathrm{cl}}^{\max}$ of the corresponding classical dynamics. Comparing Fig. 10 with Fig. 4, we observe that the chaotic motion regime of the classical dynamics corresponds to the incoherent motion regime of the quantum dynamics in the phase diagrams. Similarly the coherent motion regime corresponds to the regular motion regime. Therefore we find rough coincidence of classical regular (chaotic) motion and quantum coherent (incoherent) motion. However, note that quantum-mechanical incoherent motion appears for the parameter combinations which correspond to the regular motion regime because the incoherent motion regime is wider than the cha-

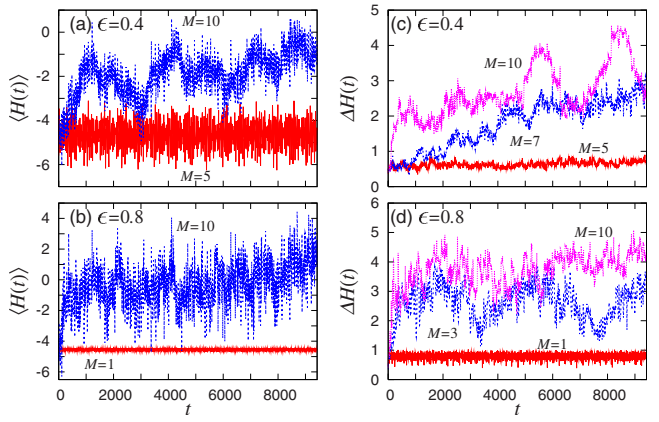

FIG. 11. (Color online) The M dependence of the expectation value $\langle H(t)\rangle$ and the standard deviation $\Delta H(t)$ of the Hamiltonian as a function of time t for various ϵ's. (a) $\langle H(t)\rangle$ in the case $\epsilon=0.4$ with $M=5$ and 10. (b) $\langle H(t)\rangle$ in the case $\epsilon=0.8$ with $M=1$ and 10. (c) M dependence of $\Delta H(t)$ in the case $\epsilon=0.4$ with $M=5,7$, and 10. (d) $\Delta H(t)$ in the case $\epsilon=0.8$ with $M=1,3$, and 10.

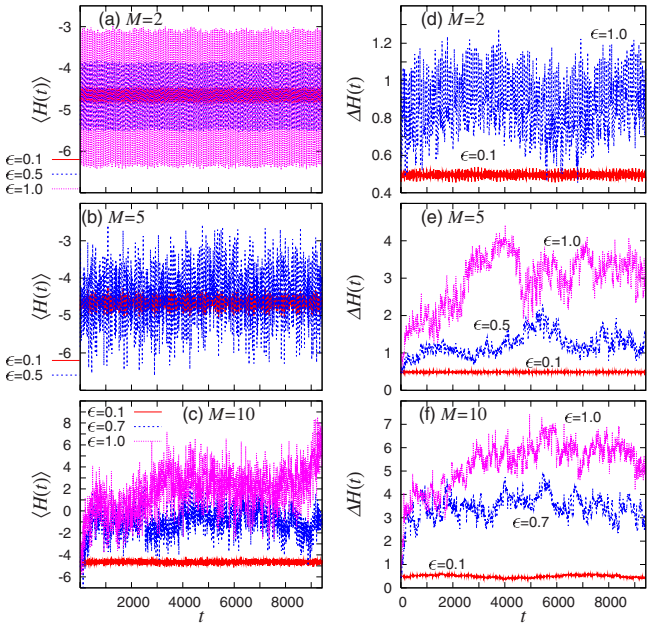

FIG. 12. (Color online) The ϵ dependence of the expectation value $\langle H(t)\rangle$ and the standard deviation $\Delta H(t)$ of the Hamiltonian as a function of time t for various M's. (a) $\langle H(t)\rangle$ in case $M=2$ with $\epsilon=0.1$, 0.5, and 1.0; (b) $\langle H(t)\rangle$ in case $M=5$ with $\epsilon=0.1$ and 0.5; (c) $\langle H(t)\rangle$ in case $M=10$ with $\epsilon=0.1$, 0.7, and 1.0; (d) $\Delta H(t)$ in case $M=2$ with $\epsilon=0.1$ and 1.0; (e) $\Delta H(t)$ in case $M=5$ with $\epsilon=0.1$, 0.5 and 1.0; (f) $\Delta H(t)$ in case $M=10$ with $\epsilon=0.1$, 0.7 and 1.0. (a) The curve representing the case $\epsilon=0.1$ is hidden rectangularly by the curve representing the case $\epsilon=0.5$, and the curve representing the case $\epsilon=0.5$ is hidden rectangularly by the curve representing the case $\epsilon=1.0$.

otic motion regime. We revisit the point later relating the spread of a wave function to the chaotic property of the corresponding classical dynamics.

Before closing the section, we give a comment on a measure of coherence. We use the degree of coherence ΔP_{L} to measure coherence instead of the widely used quantity such as fidelity [34,35] because we are interested in the relationship between transition probability and coherence of the dynamics. See Appendix C for the consistency between degree of coherence and fidelity in the present system.

V. ENERGY ABSORPTION, ENERGY SPREAD, AND COHERENCE OF THE DYNAMICS

In this and the next sections, we consider how the property of quantum dynamics in a different regime manifests itself in the corresponding wave function, emphasizing the time dependence of the expectation value and the standard deviation of the Hamiltonian, uncertainty product, and Hushimi representation. Through this consideration, the classification of the dynamics based on the degree of the coherence Eq. (15) is justified.

We first consider quantities about energy, in order to estimate energy absorption and energy spread. We deal with the expectation value $\langle H(t)\rangle$ and the standard deviation $\Delta H(t)$ of the Hamiltonian which are defined by

$$\langle H(t)\rangle \equiv \langle \psi(t)|H(t)|\psi(t)\rangle, \tag{16}$$

$$\Delta H(t) \equiv \sqrt{\langle [H(t)-\langle H(t)\rangle]^2\rangle}, \tag{17}$$

where $\langle\cdots\rangle$ denotes quantum-mechanical average. Figures 11 and 12 show time dependence of $\langle H(t)\rangle$ and $\Delta H(t)$ for various combinations of the perturbation parameters.

It is worth making a comment on $\Delta H(t)$. As shown in Table I, the energy difference ΔE^0_{02} between the ground state doublet and the first excited one is nearly equal to 2.5, i.e., $\Delta E^0_{02}\simeq 2.5\equiv \Delta H_{\mathrm{c}}$ in the unperturbed system. We can see that the two-level approximation, Eq. (14), works well for $\Delta H(t)<\Delta H_{\mathrm{c}}$.

A. Behavior of $\langle H(t)\rangle$ and $\Delta H(t)$ in the coherent motion regime

We give features of time dependence of $\langle H(t)\rangle$ and $\Delta H(t)$ in the coherent motion regime. For instance, when $M=5$ with $\epsilon=0.4$ shown in Fig. 11(a) and when $M=1$ with $\epsilon=0.8$ shown in Fig. 11(b), $\langle H(t)\rangle$ oscillates around the initial value not exceeding the energy of the top of the potential barrier. In Fig. 12(a), the time dependence of $\langle H(t)\rangle$ is shown when $M=2$ with several perturbation strengths. In this case, for each perturbation strength, $\langle H(t)\rangle$ shows similar time dependence to the above cases $M=5$ with $\epsilon=0.4$ and $M=1$ with $\epsilon=0.8$. As the perturbation strength increases, the oscillation amplitude becomes larger because the potential well become deeper. There is no substantial difference in the time dependence of $\langle H(t)\rangle$ even in case $M=5$ shown in Fig. 12(b).

In the coherent motion regime, $\langle H(t)\rangle$ shows the recurrent time dependence to the initial value. This property is attributed to the coherence of the dynamics. When the two-level approximation by the ground state doublet Eq. (14) works well during the considered time interval $t\in[0,T]$, the expectation value of the Hamiltonian takes the form

$$\langle H(t)\rangle = \frac{1}{2}[E_0(t)+E_1(t)]. \tag{18}$$

We find that $\Delta H(t)$'s also show oscillatory time dependence around the initial value as shown in Figs. 11(c) and 11(d). We do not observe a significant difference between the cases $M=5$ with $\epsilon=0.4$ and $M=1$ with $\epsilon=0.8$. In these cases, the standard deviation of the Hamiltonian satisfies an inequality, $\Delta H(t)<\Delta H_c$. This is a supplemental evidence of holding the two-level approximation in Eqs. (14) and (18). The oscillatory time dependence and the holding of the inequality are also found in the other cases, as long as they belong to the coherent motion regime, for example, $M=2$, $M=5$ with $\epsilon=0.5$, and $M=10$ with $\epsilon=0.1$, which are shown in Figs. 12(d)–12(f), respectively.

It is worth noting that, as shown in Fig. 12, the effect of the polychromatic perturbation appears in $\langle H(t)\rangle$ and $\Delta H(t)$ even for relatively small ϵ when M is large. Peak values of $\langle H(t)\rangle$ when $M=5$ with $\epsilon=0.5$ become irregular compared to those when $M=2$ with $\epsilon=1.0$. In the former case, although $\Delta H(t)$ does not show recurrence to the initial value, the inequality $\Delta H(t)<\Delta H_c$ still holds. We expect that the irregular peaks of $\langle H(t)\rangle$ appear when $\Delta H(t)<\Delta H_c$ without the recurrence to the initial value. Emergence of irregular peaks indicates that the time dependence obtains another dominant time scale which changes coherent into incoherent motion.

B. Behavior of $\langle H(t)\rangle$ and $\Delta H(t)$ in the incoherent motion regime

We next consider the time dependence of $\langle H(t)\rangle$ and $\Delta H(t)$ in the incoherent motion regime, as well as quasicoherent motion. These features are quite different from those in the coherent motion regime.

When $\epsilon=0.4$ with $M=10$ shown in Fig. 11(a), we see energy absorption of the system from the external field. This energy absorption occurs in short time $t\lesssim 1000$ at which $\langle H(t\simeq 1000)\rangle\simeq -2$. This suggests that the adiabatic transition occurs from the ground state doublet to the first excited one, because the first excited doublet of the unperturbed system has almost the same value, i.e., $E_2^0\cong E_3^0\simeq -2$ as shown in Table I. After the energy absorption, for time $t\gtrsim 1000$, $\langle H(t)\rangle$ fluctuates irregularly in the range $-5\lesssim\langle H(t)\rangle\lesssim 0$. The lower and upper bounds agree with the energy values of the ground state doublet and the top of the potential barrier, respectively. Therefore, after the energy absorption, the wave function does not remains at an instantaneous eigenstate of $H(t)$ in the sense that the state cannot be described by a simple linear combination of a few eigenstates such as Eq. (14).

With the increase of the perturbation strength, as shown in Figs. 11(b) and 12(c), the time dependence of $\langle H(t)\rangle$ becomes more irregular in the following senses: (i) energy absorption occurs in shorter time, (ii) the mean value of the fluctuation after the energy absorption becomes larger, (iii) the amplitude of the fluctuation becomes larger. These facts suggests the breakdown of the two-level approximation of Eq. (14) in the incoherent motion regime.

The time dependence of $\Delta H(t)$ in cases $M=7$ and $M=10$ with $\epsilon=0.4$ is shown in Fig. 11(c). We see that $\Delta H(t)$'s deviate from the initial values and increase with time. Similar time dependence is already seen in that of $\langle H(t)\rangle$ for incoherent motion. Especially when $M=10$ with $\epsilon=0.4$, $\Delta H(t)$ fluctuates irregularly after the rapid increase in short time, $t\lesssim 1000$. This time agrees with the energy absorption seen in $\langle H(t)\rangle$. Moreover in Fig 11(c), we find that larger M brings more rapid increase of $\Delta H(t)$, comparing the case $M=7$ to that $M=10$. As seen in Fig. 11(d) and Fig. 12(f), when $M=10$ with somewhat large ϵ, $\Delta H(t)$ also deviates from the initial value with irregular fluctuation after the rapid increase. As the perturbation strength increases, $\Delta H(t)$ varies over a wider range and behaves more irregularly with respect to time. After the increase of $\Delta H(t)$, we confirm a clear breakdown of the two-level approximation because the wave function involves several higher energy eigenstates of $H(t)$ satisfying $\Delta H(t)\gtrsim 2.5$.

As a result, in the incoherent motion regime, because $\langle H(t)\rangle>0$ and $\Delta H(t)>\Delta H_c$, the two-level approximation by the ground state doublet Eq. (14) does not work any more.

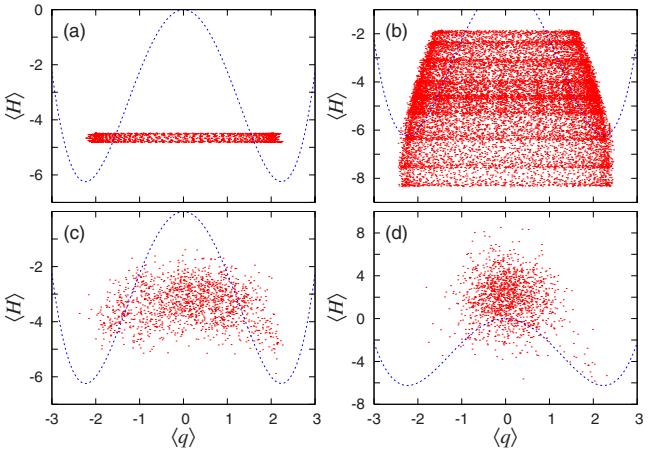

FIG. 13. (Color online) Plot of $\langle H\rangle$ as a function of $\langle q\rangle$ for various combinations of the perturbation parameters. The plots are taken at times $t=2\pi n/\Omega_1$ $(n=1,2,3,\ldots)$. The parameter combinations are (a) $M=2$, $\epsilon=0.1$; (b) $M=2$, $\epsilon=1.0$; (c) $M=10$, $\epsilon=0.3$; (d) $M=10$, $\epsilon=1.0$. The unperturbed double-well potential is drawn by the broken line as a guide to the eyes.

C. Tunneling versus pseudoactivation

In the incoherent motion regime, a wave function delocalizes over the potential barrier because of the energy absorption as mentioned in Sec. V B. We refer to this type of traveling of a wave function to *pseudoactivation* as opposed to tunneling.

In order to see competition between tunneling and pseudoactivation, we plot the expectation value of the Hamiltonian $\langle H(t)\rangle$ as a function of the expectation value of the position operator $\langle q\rangle\equiv\langle\psi(t)|q|\psi(t)\rangle$ in Fig. 13.

In the coherent motion shown in Figs. 13(a) and 13(b), the points are distributed regularly under the potential barrier with a certain width corresponding to the amplitude of oscillation of $\langle H(t)\rangle$ seen in Figs. 11 and 12. From the regular distributions, we can confirm tunneling of the wave packet between the wells.

On the contrary, in quasicoherent motion shown in Fig. 13(c), the distribution of the points seems random compared to the previous cases shown in Figs. 13(a) and 13(b). Al-

TABLE II. Classification of $\langle H(t)\rangle$, $\Delta H(t)$, $\langle H(t)\rangle+\Delta H(t)$, $\Delta q(t)\Delta p(t)$, and $\rho_{\mathrm{H}}(x,p,t)$ for each type of motion. Here $\Delta q(t)\Delta p(t)$ and $\rho_{\mathrm{H}}(x,p,t)$ are discussed in Sec. VI. A blank indicates a situation that a clearcut criterion is not found.

	Coherent motion	Quasicoherent motion	Incoherent motion
$\langle H(t)\rangle$	$\langle H(t)\rangle \lesssim -4$	$\langle H(t)\rangle \sim 0$	$\langle H(t)\rangle > 0$
$\Delta H(t)$	$\Delta H(t) \lesssim \Delta H_c$		$\Delta H(t) \gtrsim \Delta H_c$
$\langle H(t)\rangle+\Delta H(t)$	$\langle H(t)\rangle+\Delta H(t) < 0$	$\langle H(t)\rangle+\Delta H(t) \sim 0$	$\langle H(t)\rangle+\Delta H(t) > 0$
$\Delta q(t)\Delta p(t)$	$\Delta q(t)\Delta p(t) \lesssim (\Delta q \Delta p)_{\mathrm{c}}$		$\Delta q(t)\Delta p(t) \gtrsim (\Delta q \Delta p)_{\mathrm{c}}$
$\rho_{\mathrm{H}}(x,p,t)$	localized in a potential well with symmetry		delocalized over the potential barrier

though the points are not found above the potential barrier, the adiabatic transition from the ground state doublet to the first excited one is confirmed, because $\langle H\rangle$ satisfies $-5 \lesssim \langle H\rangle \lesssim -2$ whose lower and upper bounds correspond to the energy of the ground state doublet and that of the first excited one, respectively. We expect that the adiabatic transition induces the observed randomness of the distribution. In incoherent motion, as shown in Fig. 13(d), the energy values are frequently found over the top of the energy barrier. This implies that pseudoactivation of the wave function is dominant.

From the consideration of Secs. V A and V B, we can relate the types of traveling of a wave function to those of motion as follows. In the coherent motion regime, because the energy satisfies $\langle H(t)\rangle+\Delta H(t) < 0$, tunneling is the dominant process of wave packet traveling between the potential wells. On the other hand, in the incoherent motion regime, pseudoactivation is dominant to tunneling, because the energy satisfies $\langle H(t)\rangle > 0$ with large $\Delta H(t)$. The pseudoactivation is much more dominant as wave packet dynamics becomes irregular. In quasicoherent motion, we cannot clearly assign the type of traveling to either tunneling or pseudoactivation because $\langle H(t)\rangle \simeq 0$ or $\langle H(t)\rangle+\Delta H(t) \simeq 0$. This is adequate to describe the transitional character of the quasicoherent motion.

D. Summary and discussion

Behavior of the time dependence of $\langle H(t)\rangle$ and $\Delta H(t)$ changes from oscillation around the initial values to irregular fluctuation around a certain value, according to the transition from coherent motion to the incoherent one.

In the coherent motion regime, the two-level approximation by the ground state doublet describes the time evolution of a wave function, because $\langle H(t)\rangle$ and $\Delta H(t)$ oscillate regularly around the initial values with keeping $\langle H(t)\rangle < 0$ and $\Delta H(t) < \Delta H_c$. This indicates that the wave packet tunnels between the potential wells owing to coherence of the dynamics. On the other hand, in the incoherent motion regime, $\langle H(t)\rangle$ and $\Delta H(t)$ show irregular fluctuation after the rapid increases. A tendency of recurrence to the initial value is not observed in $\langle H(t)\rangle$ and $\Delta H(t)$. In Table II we summarize classification of the behavior of $\langle H(t)\rangle$ and $\Delta H(t)$ which characterize the types of motion.

In the incoherent motion regime, rapid absorption of the energy comes from resonance. It is considered that the increase of ϵ and/or M makes a resonance structure complicated and easy to happen resonances, even if we set the perturbation frequencies Ω_i's as the off resonant. The resonance appears at the small vicinity around the (primary) classical resonance, if the perturbation strength is small, as seen in Appendix A. Note that in the corresponding classical dynamics, increase of ϵ and/or M brings global chaotic behavior due to overlapping resonance.

The increase of $\Delta H(t)$ makes mutual relationship between the expanding coefficients in Eq. (7) complicated, and breaks the two-level approximation by the ground state doublet for the dynamics. In other words, difficulty of constructive interference leads to the transition in the quantum dynamics from coherent motion to incoherent motion.

It should be mentioned that we have confirmed that the growth of $\langle H(t)\rangle$ and $\Delta H(t)$ are bounded even in the incoherent motion regime. Therefore, the wave function is confined in a small subspace spanned by several instantaneous eigenstates of the Hamiltonian. The bounded-growth is a different point from the dynamics under a stochastic perturbation (see Appendix B).

VI. UNCERTAINTY PRODUCT AND HUSHIMI REPRESENTATION

In this section we consider the time dependence of the uncertainty product as the spread of a wave packet in the phase space, i.e.,

$$\Delta q(t)\Delta p(t) \equiv \sqrt{\langle (q-\langle q\rangle)^2\rangle}\sqrt{\langle (p-\langle p\rangle)^2\rangle}, \tag{19}$$

which can be used for a measure of quantum fluctuation. For instance, enhancement of the uncertainty due to the classical chaos is discussed in Ref. [36]. However, note that this quantity is not always a good measure of the phase space volume of a wave packet because this may give overestimation due to the squeezing of the wave packet [37].

Figure 14 shows the time dependence of the uncertainty product for several combinations of the strength ϵ and the number M of frequency components of the perturbation. The initial value is $\Delta q(t=0)\Delta p(t=0)=\hbar/2=0.5$ for a Gaussian packet in each case.

We also consider the Hushimi representation of a wave function $|\psi(t)\rangle$,

$$\rho_{\mathrm{H}}(x,p,t) \equiv \frac{1}{2\pi}|\langle \phi_{xp}|\psi(t)\rangle|^2, \tag{20}$$

where

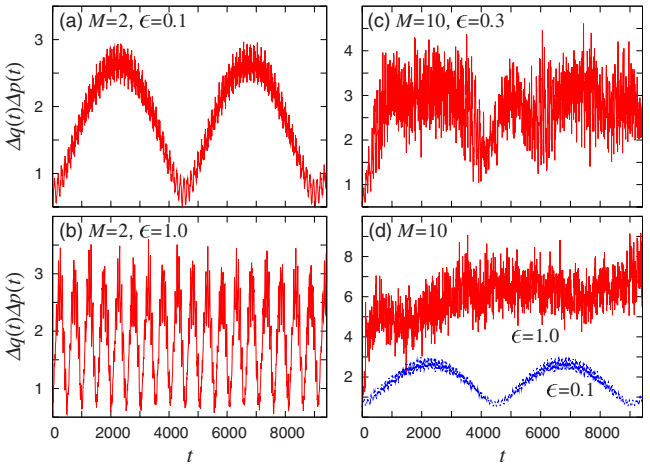

FIG. 14. (Color online) Time dependence of the uncertainty product $\Delta q(t)\Delta p(t)$ for coherent and incoherent motion. The perturbation parameters are (a) $M=2$, $\epsilon=0.1$; (b) $M=2$, $\epsilon=1.0$; (c) $M=10$, $\epsilon=0.3$; (d) $M=10$, $\epsilon=0.1$, and 1.0.

$$\phi_{xp}(q) = \left[\frac{1}{2\pi(\Delta x)^2}\right]^{1/4}\left[ipq - \frac{(q-x)^2}{4(\Delta x)^2}\right] \tag{21}$$

is a minimum uncertainty Gaussian wave packet centered at (x,p) with the variance Δx [38]. We set $\Delta x=1$ for numerical calculation. Figure 15 shows snapshots of the Hushimi representation for typical cases of coherent, quasicoherent, and incoherent motion.

We furthermore give plots of the expectation value of the momentum operator $\langle p\rangle$ as a function of the expectation value of the position operator $\langle q\rangle$ in Fig. 16. In the plots, the combinations of the perturbation parameters are the same to those in Fig. 13.

A. Behavior of $\Delta q(t)\Delta p(t)$ and $\rho_H(x,p,t)$ in the coherent motion regime

When $M=2$ with $\epsilon=0.1$ as shown in Fig. 14(a), $\Delta q(t)\Delta p(t)$ shows oscillatory time dependence with recurrence to the initial value. For the initially localized state in the right well of the potential, $\Delta q(t)\Delta p(t)$ grows with time because a tail of the wave packet leaks out. At $t \simeq T/2 \simeq 4.5\times 10^3$, the wave function localizes in the opposite well by tunneling, then the uncertainty product becomes small again, $\Delta q(T/2)\Delta p(T/2) \simeq \Delta q(0)\Delta p(0)$. As shown in Fig. 14(b), even for larger perturbation strength $\epsilon=1.0$, $\Delta q(t)\Delta p(t)$ oscillates with recurrence to the initial value. Increase of the perturbation strength enhances the frequency of oscillation of $\Delta q(t)\Delta p(t)$ as well as in $P_L(t)$, $\langle H(t)\rangle$, and $\Delta H(t)$.

In the coherent motion regime, a wave function has localization property which brings the tunneling of the wave packet. As confirmed in the Hushimi representation of a state shown in Figs. 15(a) and 15(b), contour lines are localized around the center of a potential well with symmetry. Even at the final time T, the wave function can localize with symmetry in the opposite well.

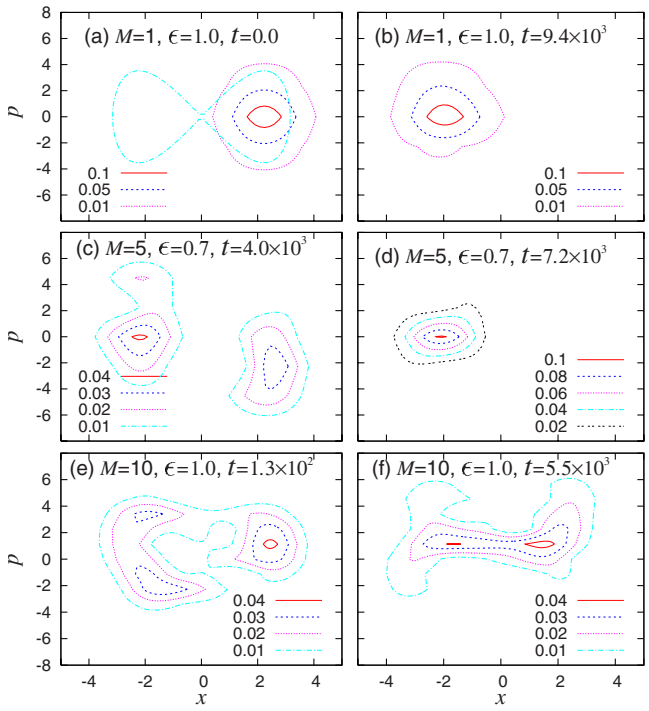

FIG. 15. (Color online) Snapshots of the Hushimi representation for typical cases of the three types of motion. The curve of the figure eight in (a) indicates the unperturbed separatrix. (a) and (b) represent cases corresponding to coherent motion. Contour lines of the Hushimi representation of the initial wave packet, Eq. (9), are shown in (a). The time in (b) is the final time T. (c) and (d) represent cases of quasicoherent motion. The contour plots in (c) and (d) are taken at the times which satisfy $P_L(t) \simeq 0.5$ and 0.7, respectively. (e) and (f) represent cases corresponding to a typical incoherent motion. The times in (e) and (f) are those which satisfy $P_L(t) \simeq 0.7$ in both cases.

We also confirm coherence of the dynamics in the $(\langle q\rangle, \langle p\rangle)$ plot shown in Fig. 16. In Fig. 16(a) the points are distributed regularly in the range $-2 \leqslant \langle q\rangle \leqslant 2$ with $\langle p\rangle \simeq 0$ owing to tunneling. As ϵ and/or M increase, the points form a structure with diagonally right down because the centroid motion of the wave packet becomes dominant.

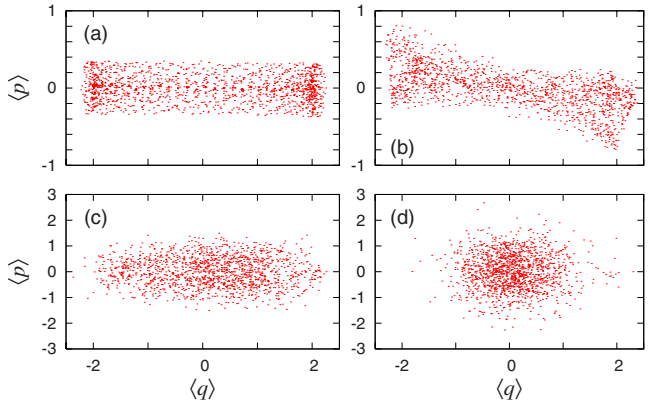

FIG. 16. (Color online) Plot of $\langle p\rangle$ as a function of $\langle q\rangle$ for various cases. The combination of the perturbation parameters are the same in Fig. 13.

B. Behavior of $\Delta q(t)\Delta p(t)$ and $\rho_{\mathrm{H}}(x,p,t)$ in the incoherent motion regime

When $M=10$ with relatively large perturbation strength $\epsilon \gtrsim 0.3$ shown in Figs. 14(c) and 14(d), the oscillatory time dependence of $\Delta q(t)\Delta p(t)$ is not found any more. The time dependence of $\Delta q(t)\Delta p(t)$ show irregular fluctuation around a certain value after deviation from the initial value. The time dependence is similar to those of $\langle H(t)\rangle$ and $\Delta H(t)$. In the cases, a wave function cannot return to the initial shape within the time interval T once the wave function delocalizes over the potential barrier. This tendency becomes stronger with the increase of the perturbation strength.

The delocalization of a wave function in the phase space is clearly seen through the Hushimi representation in Figs. 15(e) and 15(f). Moreover, even though $P_{\mathrm{L}}(t)$'s have almost the same value, the Hushimi representations show quite different shapes with one another. We also confirm that the wave function does not clearly split into two parts, each of which localizes around centers of the potential wells.

In the quasicoherent motion shown in Figs. 15(c) and 15(d), it is shown that a wave packet keeps the localization property in the space without clear symmetry.

C. Summary and discussion

In the coherent motion regime, $\Delta q(t)\Delta p(t)$ shows regular oscillatory time dependence with recurrence to the initial value due to coherence of the dynamics. On the other hand, in the incoherent motion regime $\Delta q(t)\Delta p(t)$ shows irregular fluctuation after deviation from the initial value because of decoherence.

From Fig. 14, a critical value $(\Delta q\Delta p)_{\mathrm{c}} \sim 3.5$ exists above which time dependence of $\Delta q(t)\Delta p(t)$ loses recurrent behavior and begins to fluctuate around a certain value. This value may corresponds to the height of the unperturbed separatrix $p(q=\sqrt{a}, E=0) \simeq 3.5$. This suggests that quantum dynamics loses coherence when the wave function leaks out onto the classical separatrix, especially in the p direction. Indeed we confirmed that the recurrent time dependence to the initial value of the quantities such as $\Delta q(t)\Delta p(t)$, $\langle H(t)\rangle$, and $\Delta H(t)$ is not broken against the increase of ϵ and M in a *single* well system, which is described by changing the sign of the parameter a in Eq. (3) as $V_0(q)=q^4/4+aq^2/2$.

Finally, we here reconsider the disagreement between the phase diagram of the quantum dynamics and that of the corresponding classical one, mentioned in the end of Sec. IV. We take the following three factors into account: (i) the initial position of a wave packet for tunneling, (ii) the area of regular region in the classical phase space, and (iii) the spread of a wave function.

The initial position of a wave packet in the phase space is a very important factor for tunneling [1]. If the initial position is taken in the chaotic sea, the wave packet dissolves in the sea as time evolves and does not show tunneling between the Kolmogorov-Arnold-Moser tori.

Generally speaking, as the perturbation strength increases, the stochastic layer becomes wider and finally the whole region of the phase space becomes chaotic. In our system, we expect that the larger number of the frequency components brings the stronger growth of the stochastic layer, when the perturbation strength is fixed. Therefore, as M and/or ϵ increase, the area of the regular region supporting tori, which is responsible for the tunneling, decreases, and finally a torus disappears [26].

Global phase space structure influences quantum-mechanical behavior because a wave packet has the natural tendency to spread over the space [19]. Therefore, even if an initial wave packet is taken in a regular region of the phase space, a tail of the wave function is likely to leak out into the stochastic layer around the classically regular region as time evolves.

Coexistence of the above three factors suggests that the quantum motion can become irregular even when the corresponding classical motion is regular. We expect that this coexistence is the origin of the disagreement of the phase diagrams seen in Figs. 4 and 10.

VII. QUANTUM-CLASSICAL CORRESPONDENCE IN TERMS OF THE WIGNER FUNCTION

In this section we consider quantum-classical correspondence in terms of the Wigner function and its negativity. The Wigner function of a system is defined by

$$\rho_{\mathrm{W}}(q,p,t) \equiv \frac{1}{2\pi}\int_{-\infty}^{\infty} \left\langle q-\frac{x}{2}\middle|\rho(t)\middle|q+\frac{x}{2}\right\rangle e^{i2\pi x}dx, \quad (22)$$

where $\rho(t) \equiv |\psi(t)\rangle\langle\psi(t)|$ is the density operator. The Wigner function is often used to investigate quantum-classical correspondence because the function gives the same form of an expectation value to the corresponding classical one. However, the Wigner function cannot be directly considered as probability density because it is not positive definite, different from the Hushimi representation which is always positive definite due to Gaussian coarse graining [38].

In order to consider quantum-classical correspondence, we introduce the classical phase space density $\rho_{\mathrm{cl}}(q,p,t)$ which obeys the Liouville equation. The formal solution is

$$\rho_{\mathrm{cl}}(q,p,t) = \int dq_0 dp_0 \delta[q-q(q_0,p_0;t)] \times \delta[p-p(q_0,p_0;t)]\rho_{cl}(q,p,t=0), \quad (23)$$

where $\delta(x)$ is Dirac delta function, $[q(q_0,p_0;t), p(q_0,p_0;t)]$ is the time-evolved classical phase space coordinate at time t starting from the initial condition (q_0,p_0), and $\rho_{\mathrm{cl}}(q,p,t=0)$ is the initial phase space density [39]. For comparison of the time evolution of the Wigner function with that of the classical phase space density, we set $\rho_{\mathrm{cl}}(q,p,t=0)$ as the Wigner representation of the quantum initial state of Eq. (9),

$$\rho_{\mathrm{cl}}(q,p,t=0) = \frac{1}{\pi}\exp\left[-\frac{(q-q_0)^2}{\sigma} - \sigma p^2\right]. \quad (24)$$

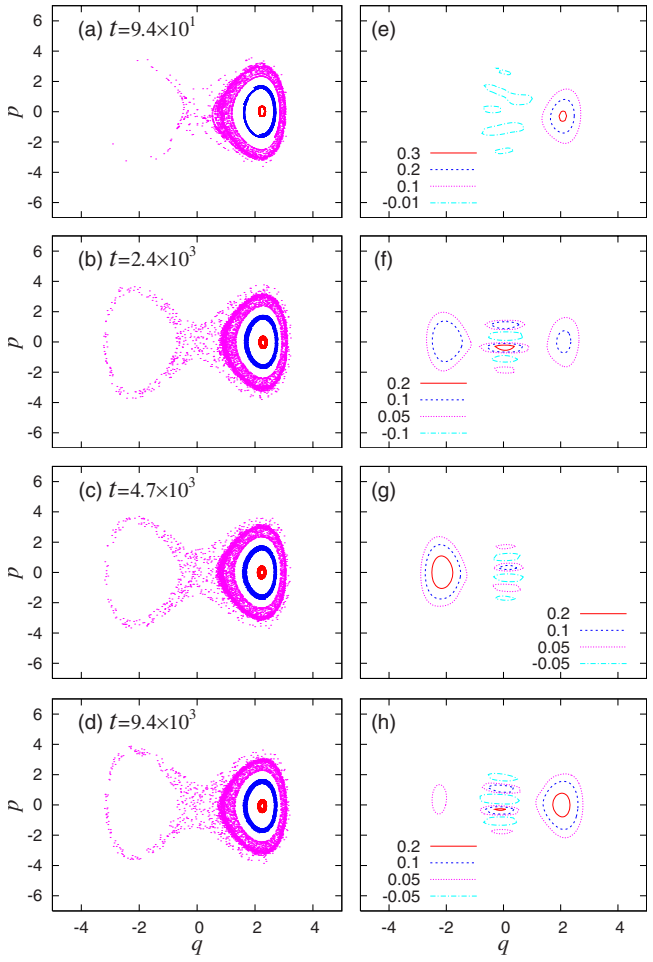

FIG. 17. (Color online) Time evolution of the classical phase space density $\rho_{\mathrm{cl}}(q,p,t)$ (left column) and the Wigner function $\rho_{\mathrm{W}}(q,p,t)$ (right column) in the case $M=2$ with $\epsilon=0.2$. The classical phase space density is denoted by three contour lines $\rho_{\mathrm{cl}}(q,p,t)\simeq 3.076\times 10^{-1}$, 1.360×10^{-1}, and 2.026×10^{-2}, from the inside to the outside. The most outside contour line is set at the vicinity of the unperturbed separatrix.

A. Quantum-classical correspondence in terms of the Wigner function

We here consider dynamics of the Wigner function comparing it with the corresponding classical dynamics for typical coherent and incoherent motion.

Figure 17 shows the time evolution of the classical phase space density of Eq. (23) and the Wigner function of Eq. (22) in the case $M=2$ with $\epsilon=0.2$ that belongs to the regular motion regime in the classical dynamics and the coherent motion regime in the quantum dynamics, respectively. We first consider the classical dynamics. In Fig. 17 the most outside contour line of the classical phase space density exists at the vicinity of the unperturbed separatrix at the initial time. From the classical dynamics shown in Fig. 17, we see the existence of somewhat large stable islands around the stable fixed points of the unperturbed system. Inside of the right stable island, the phase space density becomes wider as time evolves because of the whorl structure [39,40]. On the other hand, we see that the stochastic layer grows rather weakly in the time evolution. In the quantum dynamics, we see that coherent tunneling takes place between the classical stable regions without leaking of a wave function into the outside of the classical stochastic layer. We also confirm the property that the wave function can localize inside of either potential well. It is remarkable that the Wigner function takes negative values around the unstable fixed point $(q,p)=(0,0)$ because of interference of the wave function. However, this negative-value property of the Wigner function is washed away by integrating with respect to p: $|\psi(q,t)|^2=\int dp\rho_{\mathrm{W}}(q,p,t)$, which has a very small value around $q=0$ in the coherent motion regime.

Figure 18 shows the time evolution of the classical phase space density and the Wigner function in the case $M=7$ with $\epsilon=0.7$ that belongs to the chaotic motion regime in the classical dynamics and the incoherent motion regime in the quantum dynamics, respectively. From the left and middle columns in Fig. 18, we observe that the classical dynamics makes a fine structure in the phase space. The fine structure is formed by fast growth of both of the whorl structure around the right stable fixed point and the tendril one around the unstable fixed point within relatively short time. On the contrary, we confirm that in the quantum dynamics the wave function delocalizes irregularly over the space by the Wigner function given in the right column. The delocalization of the wave function is already shown in the Hushimi representation in Fig. 15.

B. Negativity of the Wigner function

In incoherent motion, the Wigner function takes a negative value in wide regions compared to the coherent motion. Especially at time $t\sim 4.7\times 10^3$, when the classical chaos fully developed, such regions exist on the classical stochastic layer disconnectedly and globally. On the basis of this property, we consider characterization of the difference between coherent and incoherent motion in terms of negativity N_- of the Wigner function. The negativity of the Wigner function is defined by

$$N_-(t)\equiv\int_D|\rho_{\mathrm{W}}(q,p,t)|dqdp, \tag{25}$$

where D is a region in which the Wigner function takes a negative value. The negativity of the Wigner function is also considered in order to investigate quantum-classical *transition* for a chaotic system in Ref. [41].

We give time dependence of $N_-(t)$ for several perturbation parameters in Fig. 19. In the coherent motion regime, $N_-(t)$ increases because the wave function leaks out into the outside of the potential barrier, and decreases toward zero because the wave function localizes again inside of the opposite potential well, as shown in Fig. 17. In the coherent motion regime, such recurrent time dependence is similar to that of $P_{\mathrm{L}}(t)$, $\langle H(t)\rangle$, $\Delta H(t)$, and $\Delta q(t)\Delta p(t)$. On the other hand, in the incoherent motion regime, $N_-(t)$ increases without the recurrence and eventually fluctuates around a certain value because of the delocalization of the wave function as shown in Fig. 18. In the incoherent motion regime, such property of the time dependence is similar to $P_{\mathrm{L}}(t)$, $\langle H(t)\rangle$,

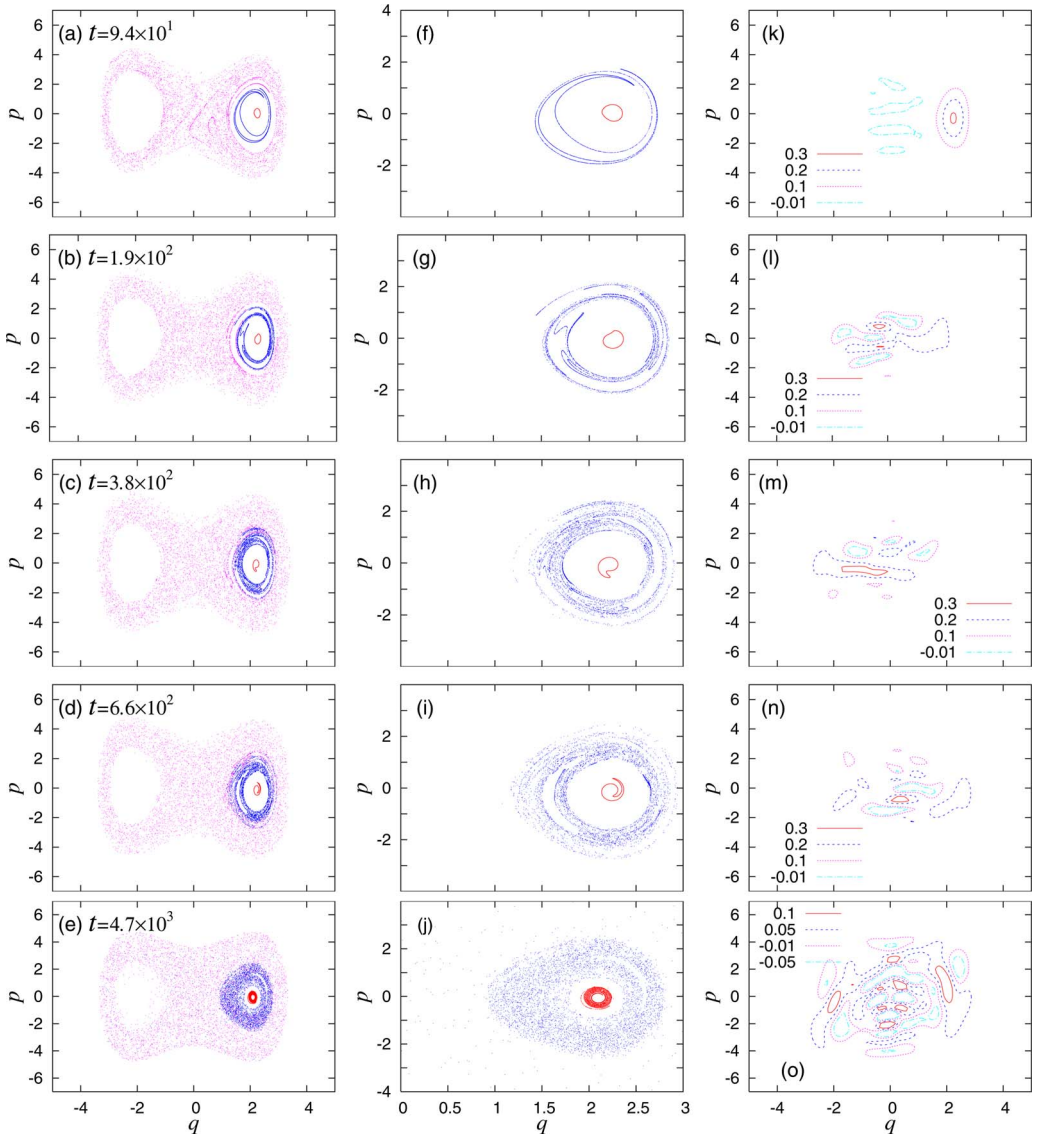

FIG. 18. (Color online) Time evolution of the classical phase space density $\rho_{\mathrm{cl}}(q,p,t)$ (left and middle columns) and the Wigner function $\rho_{\mathrm{W}}(q,p,t)$ (right column) in the case $M=7$ with $\epsilon=0.7$. The values of the contour lines in the left column are the same as Fig. 17. The middle column represents the two inner contour lines shown in the left column.

$\Delta H(t)$, and $\Delta q(t)\Delta p(t)$. In other words, we can see that this behavior observed in the $N_{-}(t)$ well corresponds to the change of motion discussed in Secs. IV–VI.

Figure 20 shows the perturbation parameter dependence of minimum of N_{-} for the several numbers of the frequency components, where the minimum of N_{-} has been taken for relatively large time. We clearly find that the minimum of N_{-} increases as ϵ and/or M increase. Moreover it should be noted that the minimum of N_{-} in the polychromatically perturbed cases approaches to that in the stochastically perturbed one with increase of M.

VIII. DECOHERENCE IN A KICKED DOUBLE-WELL SYSTEM

In this section we confirm whether the decoherence phenomenon of the quantum dynamics can be observed in a kicked double-well system,

$$H_{\mathrm{kick}}(p,q,t) = H(p,q,t) - k\cos q\sum_{n}\delta(t-n\tau), \qquad (26)$$

where the Hamiltonian $H(p,q,t)$ is given by Eq. (1). The strength and the period of the kicking impulse are given by k and τ, respectively. Hamiltonian H_{kick} keeps the symmetry mentioned in Sec. II even when the impulse exists. If the potential term in $H(p,q,t)$ is a harmonic oscillator, i.e., $V(q,t)\propto q^2$, the system becomes a kicked harmonic oscillator whose quantum-classical correspondence is well investigated [42]. We set the kicking frequency $2\pi/\tau$ as incommensurate to Ω_i's. For simplicity we consider a case with $M=1$ and $\tau=2\pi/\Omega_{10}\simeq 4.08$ in the following numerical calculations.

First we investigate the effect of a purely kicking impulse by setting $\epsilon=0$. Figure 21 shows the time dependence of $P_{\mathrm{L}}(t)$ for several kicking strengths. When the kicking strength is relatively small, $k\lesssim 3$, increase of the kicking

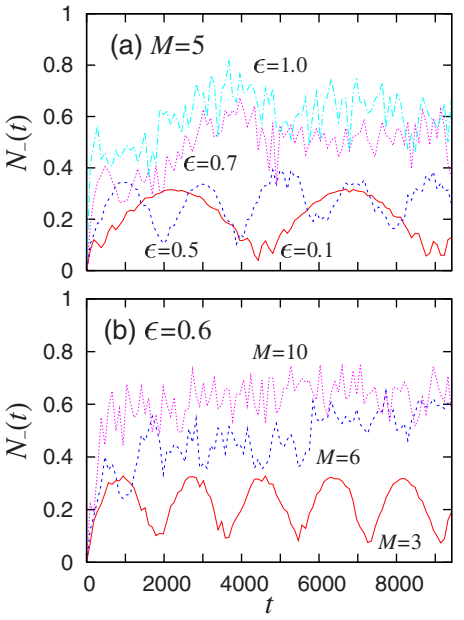

FIG. 19. (Color online) Perturbation parameter dependence of N_- as a function of time t. The perturbation strength dependence is shown in (a) when $M=5$ for $\epsilon=0.1$, 0.5, 0.7, and 1.0. The number of the frequency components dependence is shown in (b) when $\epsilon=0.6$ for $M=3$, 6, and 10.

strength enhances the frequency of coherent tunneling because of chaos assisted tunneling. As shown in Figs. 21(c) and 21(d), the coherent tunneling is broken by a further increase of the kicking strength. A critical kicking strength exists for change from coherent oscillation to irregular fluctuation.

Second we investigate influence of a sinusoidal perturbation on the kicked double-well system. Note that the system has polychromatic time dependence due to the two incommensurate frequencies, Ω_1 and $2\pi/\tau$, in the time-dependent potential. We show time-dependence of $P_L(t)$ when $k=1$ with several ϵ's in Fig. 22. Comparing Fig. 22(a) with Fig. 21(a), we see that a significant change does not occur when the strength of the sinusoidal perturbation is relatively small. On the other hand, as shown in Fig. 22(b), increase of the sinusoidal perturbation strength distorts the coherent tunneling. As the strength of the sinusoidal perturbation increases further, $P_L(t)$ is distorted toward decoherence. As shown in

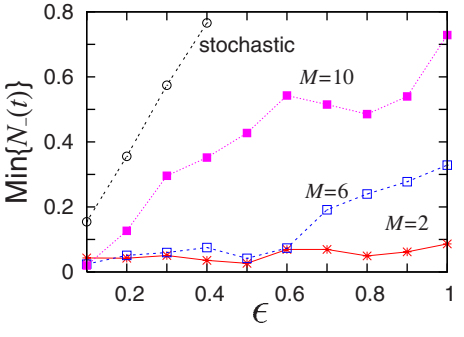

FIG. 20. (Color online) Perturbation strength dependence of the minimum of N_-. The minimum of N_- is taken as $t \geq 4500$.

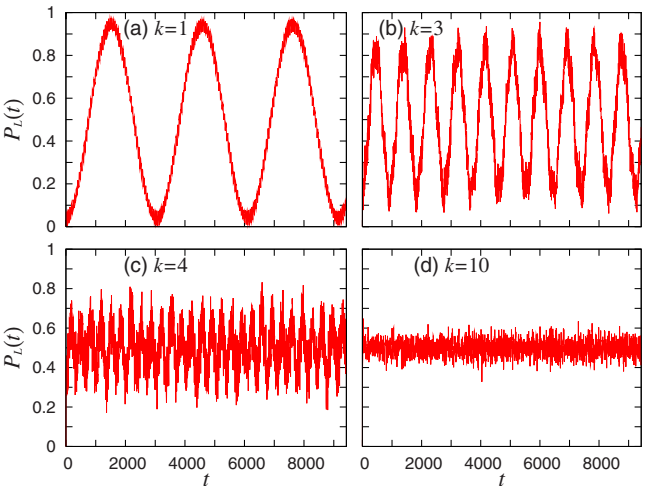

FIG. 21. (Color online) Time dependence of $P_L(t)$ for the kicked double-well system, Eq. (26), with $\epsilon=0$.

Fig. 22(d), we have confirmed occurrence of decoherence of the quantum dynamics when the strength of the sinusoidal perturbation is large, $\epsilon \gtrsim 2.0$.

IX. SUMMARY

In the present paper, we numerically studied quantum dynamics as well as the corresponding classical dynamics in a one-dimensional double-well system which is parametrically driven by a polychromatic perturbation. The time-dependent perturbation consists of M sinusoidal modes with the strength ϵ. Each frequency of the modes is mutually incommensurate and off resonant to the intrinsic time scale of the unperturbed system. We summarize the results as follows:

(i) We have classified the type of motion in the quantum dynamics into coherent and incoherent motion, on the parameter space. For the classification, we introduced a quantity, i.e., degree of coherence, to measure regularity of time

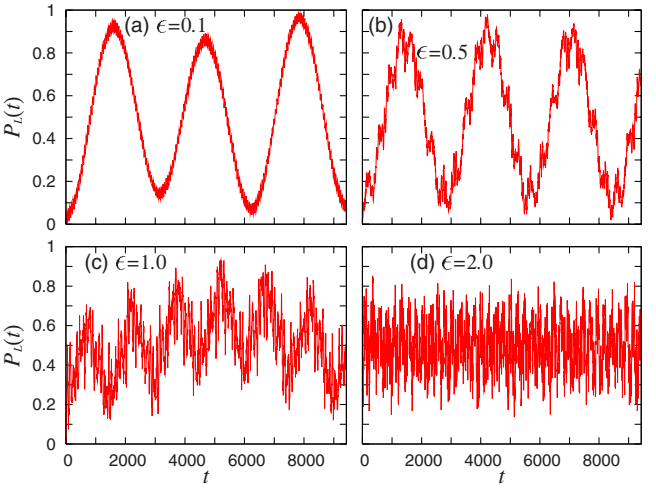

FIG. 22. (Color online) Time dependence of $P_L(t)$ for the kicked double-well system, Eq. (26), with $M=1$. The kicking strength is $k=1$.

dependence of transition probability between the wells. As the strength and/or the number of the perturbation increase, coherent motion changes into an incoherent one when $M \geqslant 3$. There exists the critical value $\epsilon_c(M)$ of the perturbation strength, above which the transition from coherent motion to incoherent one occurs. As the number of the frequency components increases, the critical value $\epsilon_c(M)$ becomes smaller. Therefore, the polychromatic perturbation can affect the quantum dynamics even for relatively small perturbation strength.

(ii) In the coherent motion regime, $\epsilon < \epsilon_c(M)$, a wave packet still shows coherent tunneling and has the property to localize in either of the potential wells, owing to coherence of the dynamics. Two-level approximation by the ground state doublet describes well the time evolution of a wave function. Physical quantities such as the expectation value and the standard deviation of the energy, and the uncertainty product, show oscillatory time dependence with recurrence to the initial values. The frequency of the time dependence is enhanced as the perturbation strength and/or the number of frequency components increase. Negativity of the Wigner function in the regime also shows similar time dependence.

(iii) In the incoherent motion regime, $\epsilon > \epsilon_c(M)$, a wave function spreads over the potential barrier and cannot localize in either well because of decoherence caused by the perturbation. Time dependence of some physical quantities shows irregular fluctuation around a certain value after the rapid increase due to the resonance. The two-level approximation no longer holds in the regime. Moreover the energy growth is bounded at a certain value.

(iv) The classical dynamics shows regular or chaotic motion depending on the perturbation parameters. In the phase diagram of the quantum dynamics spanned by the perturbation parameters, the coherent (incoherent) motion regime approximately overlaps the regular (chaotic) motion regime in the phase diagram of the corresponding classical dynamics.

(v) Decoherence in a kicked double-well system has also been observed as the strength of the kick increases. When a sinusoidal perturbation with somewhat large strength is applied to the kicked system, the kicking strength for the docoherence becomes small compared to the purely kicked case.

(vi) We have confirmed the decoherence phenomena caused by the perturbation with resonant frequencies even when the perturbation strength is small. We also compared quantum dynamics under the polychromatic perturbation with that under a stochastic perturbation. The dynamics under the stochastic perturbation with relatively large perturbation strength also show incoherent motion as seen in the polychromatically perturbed case. However, the energy growth continues unboundedly, different from the polychromatically perturbed cases. Furthermore we have obtained a rough consistency between the decoherence phenomena based on the degree of coherence and on the decay of fidelity.

In the incoherent motion regime, we have not observed a sign that a wave function relocalizes once it delocalizes. We can make the wave packet localized in the opposite well using optimal control theory [43,44]. On the other hand, in a double-well system, control of the dynamics within an appropriate time scale can be applied to many physical and chemical processes such as intramolecular hydrogen transfer [45], isomerization [46], and so on. The detail of the relationship between decoherence in quantum dynamics and the controllability of the wave packet dynamics will be given elsewhere.

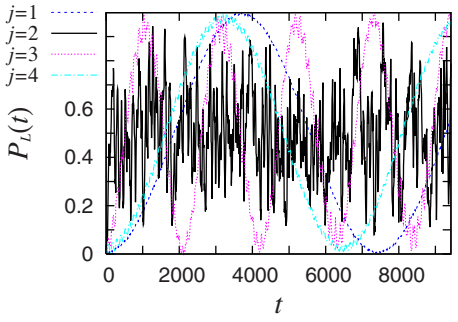

FIG. 23. (Color online) Resonance of transition probability when $M=5$ with small perturbation strength $\epsilon=0.1$. Sets of the perturbation frequencies $\{\Omega_i^{(j)}\}$ have the same width $\Omega_5^{(j)}-\Omega_1^{(j)}$ with different minimum frequency Ω_1, respectively.

ACKNOWLEDGMENT

One of the authors (A.I.) would like to thank Professor M. Goda for encouragement and discussion on this study.

APPENDIX A: TIME DEPENDENCE OF TRANSITION PROBABILITY FOR RESONANT FREQUENCIES

We give the time dependence of transition probability $P_L(t)$ under a polychromatic perturbation with resonant frequencies. It has been shown that the coherent tunneling between the wells is broken by a monochromatic perturbation $(M=1)$ with the resonant frequency when the perturbation strength is large [25].

We show that a polychromatic perturbation even with a small perturbation strength breaks the coherent tunneling. For this reason, we calculate $P_L(t)$ for some frequency sets $\{\Omega_i^{(j)}\}$, where the index $j(=1,2,\ldots)$ represents such a set of the perturbation frequencies. Numerical results are shown in Fig. 23 for four sets of $\{\Omega_i^{(j)}\}$, $j=1,\ldots,4$ when $M=5$ with $\epsilon=0.1$.

We take the frequency sets $\{\Omega_i^{(j)}\}$ with keeping $\Omega_5^{(j)}-\Omega_1^{(j)}=$const for the all sets, and take $\Omega_1^{(j=2)}=2.5\simeq\Delta E_{20}^0$; the frequency value is very close to the energy difference between the ground state doublet and first excited one of the unperturbed system (see Table I). The others have the off-resonant minimum frequency; $\Omega_1^{(j=1)}=2.0$, $\Omega_1^{(j=3)}=3.0$, and $\Omega_1^{(j=4)}=3.5$, respectively. Because of the resonance between the unperturbed system and the external field, the transition probability for the $j=2$ case shows different time dependence from the other cases, even when the perturbation strength is small. In the $j=1$ and $j=4$ cases, $P_L(t)$'s show regular oscillation similar to the unperturbed one. Moreover in the $j=3$ case, the tunneling frequency is more enhanced than the $j=1$ and $j=4$ cases. This indicates that the resonance width is narrow for a small perturbation strength.

The coherent tunneling breaks down even with a small perturbation strength in the polychromatic perturbation compared to the monochromatic one, because the resonance occurs more easily as the number of frequency components increases.

APPENDIX B: COMPARISON TO STOCHASTIC PERTURBATION

In this appendix, we show numerical results of quantum dynamics driven by a stochastic perturbation in order to compare with that driven by a polychromatic one in the text. First we explain the numerical method of our treatment for the stochastic perturbation. In the method, the time evolution of a wave function is described by Eq. (11),

$$|\psi(t+\Delta t)\rangle = \exp\left(-\frac{i}{\hbar}\frac{K}{2}\Delta t\right)\exp\left(-\frac{i}{\hbar}[V_0(q)+\xi(t)q^2]\Delta t\right) \times \exp\left(-\frac{i}{\hbar}\frac{K}{2}\Delta t\right)|\psi(t)\rangle + O(\Delta t^3). \quad \text{(B1)}$$

Here we used a simple noise process replacing the time-dependent part $A(t)/2$ of the potential, Eq. (4), by a discretized time-series $\xi(t_n)$ obeying independently identical distributed random numbers with the same power as the ploychromatically perturbed case. The autocorrelation function of $\xi(t_n)$ is given by

$$\langle \xi(t_n)\xi(t_m)\rangle \propto \delta_{mn}. \quad \text{(B2)}$$

We have also confirmed that the numerical results are almost the same when we used Gaussian distribution instead of the uniform distribution. The above treatment of a noise process $\xi(t)$ is the same as those used in a noise-added kicked system in the sense that the randomness is directly included in the time evolution operator [15,47].

It should be noted that an alternative method is used as treatment of the Schrödinger equation with stochastic time-fluctuation $\xi(t)$, i.e., *the stochastic Schrödinger equation for an open system* [48]. Then the Itô-type stochastic Schrödinger equation is given by

$$d|\psi(t)\rangle = -\frac{i}{\hbar}H_0|\psi(t)\rangle dt - \frac{i}{\hbar}V_1'(q)|\psi(t)\rangle dW - \frac{1}{2}V_1'(q)^2|\psi(t)\rangle dt. \quad \text{(B3)}$$

Here H_0 denotes the noise-free part of the Hamiltonian, $V_1'(q)$ is given through an expression $V_1(q,t)=V_1'(q)\xi(t)$, and $dW(t)=\xi(t)dt$ is a Wiener process which satisfies $\langle dW(t)\rangle = 0$ and $\langle dW(t)dW(s)\rangle = \delta(t-s)$, where $\langle\cdots\rangle$ is the ensemble average over all possible realizations of the noise. In the stochastic Schrödinger equation, V_1' represents the effect of a environment coupled to the double-well system and the parameter ϵ should rather be interpreted as a coupling constant between the system and the environment. When the parameter is very small, $\epsilon \simeq O(10^{-3})$, the quantum dynamics of the system shows good agreement with our naive treatment mentioned above (not shown). It is worth noting that the time evolution equation of the Wigner function corresponding to Eq. (B3) has a diffusive term which washes away a fine structure of the Wigner function in the phase space [41].

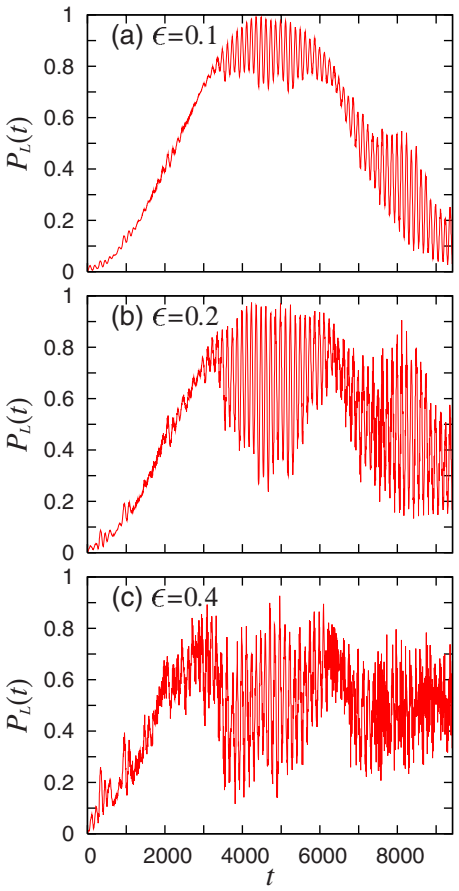

FIG. 24. (Color online) Time dependence of transition probability $P_L(t)$ under the stochastic perturbation. The perturbation strengths are (a) $\epsilon=0.1$; (b) $\epsilon=0.2$; (c) $\epsilon=0.4$.

1. Transition probability

Figure 24 shows time dependence of transition probability $P_L(t)$ under the stochastic perturbation for several perturbation strength. As shown in Fig. 24(a), until $t \lesssim 3000$, $P_L(t)$ shows similar behavior to the case $M=10$ with the same perturbation strength ($\epsilon=0.1$). However, after $t \gtrsim 3000$, fluctuation takes place in the time dependence which is quite different from the case $M=10$. The difference becomes clearer when $\epsilon=0.2$ shown in Fig. 24(b). When $\epsilon=0.4$ shown in Fig. 24(c), $P_L(t)$ shows almost linear growth with time until $t \lesssim 2000$, and irregular fluctuation in $t \gtrsim 2000$. The behavior is quite similar to the polychromatically perturbed case $M=10$ with $\epsilon=0.4$. As a result, we expect that the quantum dynamics under a polychromatic perturbation indeed approaches to that under a stochastic perturbation as the number of frequency components of the perturbation increases.

Fourier transform $I(\omega)$ of $P_L(t)$ is given in Fig. 25. Interestingly, the peaks appears at almost same values on the ω axis independent of the perturbation strength. The height of the peaks becomes closer to each other as the perturbation strength increases.

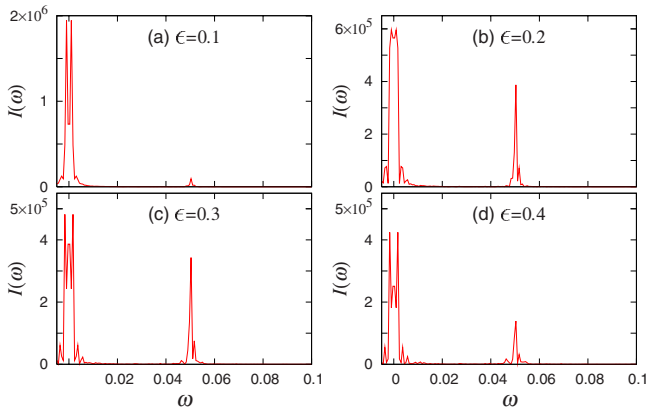

FIG. 25. (Color online) Fourier transform $I(\omega)$ of the transition probability under the stochastic perturbation for some perturbation strength ϵ's.

2. Energy absorption and energy spread

Figure 26 shows the time dependence of the expectation value and the standard deviation of the Hamiltonian under the stochastic perturbation for various perturbation strengths. When the perturbation strength is small (ϵ=0.1), $\langle H(t)\rangle$ and $\Delta H(t)$ oscillate around the initial values, respectively. We do not see substantial difference from those in the polychromatically perturbed case $M=10$ with ϵ=0.1. However, the cases with ϵ=0.3 and 0.4 show quite different time dependence from those in the polychromatically perturbed case $M=10$ with ϵ=0.3 and 0.4. In the stochastically perturbed cases, $\langle H(t)\rangle$ and $\Delta H(t)$ grow unboundedly and almost linearly in time, while they are suppressed around a certain value in the polychromatically perturbed cases. Under the stochastic perturbation, the system can continue energy absorption from the external field unboundedly [49].

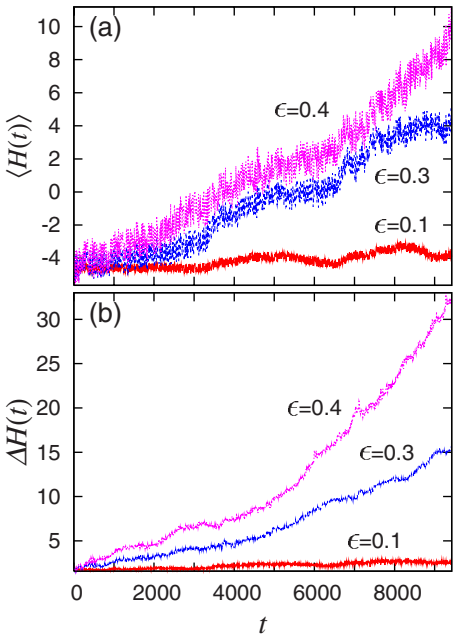

FIG. 26. (Color online) Time dependence of (a) the expectation value $\langle H(t)\rangle$, and (b) the standard deviation $\Delta H(t)$ of the Hamiltonian under the stochastic perturbation for several ϵ's.

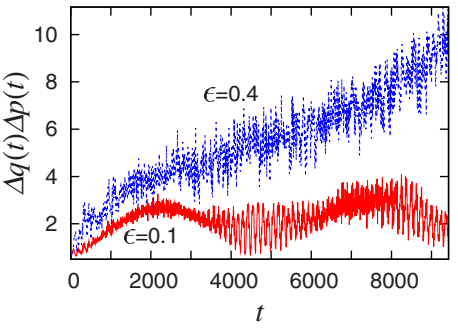

FIG. 27. (Color online) Time dependence of the uncertainty product $\Delta q(t)\Delta p(t)$ under the stochastic perturbation for some perturbation strength ϵ's.

3. Uncertainty product and Hushimi representation

Figure 27 shows time dependence of the uncertainty product $\Delta q(t)\Delta p(t)$ under the stochastic perturbation for various perturbation strengths. When ϵ is small, $\Delta q(t)\Delta p(t)$ shows recurrence to the initial value as seen in the time dependence of $\langle H(t)\rangle$ and $\Delta H(t)$. On the other hand, for relatively large perturbation strength, we can observe unbounded growth of $\Delta q(t)\Delta p(t)$ attributed to the unbounded energy absorption.

Figure 28 gives snapshots of the Hushimi representation of a wave function under the stochastic perturbation for vari-

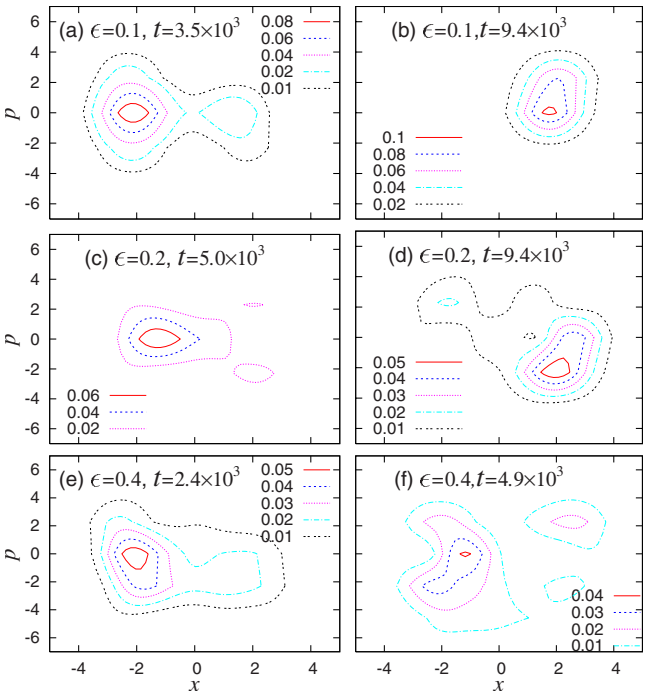

FIG. 28. (Color online) Snapshots of the Hushimi representation under the stochastic perturbation for some perturbation strengths. The perturbation strengths are ϵ=0.1 in (a) and (b); ϵ=0.2 in (c) and (d); ϵ=0.4 in the (e) and (f). The times at which the corresponding snapshot is taken are (a) $t=3.5\times10^3$, when $P_L(t)$ begins to show different time dependence from the unperturbed one; (b) $t=T$; (c) $t=5.0\times10^3$, when $P_L(t)$ begins to fluctuate; (d) $t=T$; (e) $t=2.4\times10^3$, until when $P_L(t)$ grows linearly with time; (f) $t=4.9\times10^3$, around this time $P_L(t)$ fluctuates irregularly.

ous perturbation strengths. In Fig. 28(a), the snapshot is taken when $P_L(t)$ begins to show a clear difference from the unperturbed case. We still see localization with symmetry of the wave function. However, as shown in Fig. 28(b), the symmetry is slightly distorted at the final time T. As shown in Figs. 28(c)–28(f), with an increase of the perturbation strength, a wave function spreads over the space without symmetry as time evolves.

Here we recall the difference for $t \gtrsim 3000$ between the time dependence of $P_L(t)$ in the stochastically perturbed case with $\epsilon=0.1$ and that in the unperturbed case. At first glance, one may naively think that the classical separatrix has little influence on the quantum dynamics since $\langle H(t)\rangle + \Delta H(t) < 0$ even in the stochastically perturbed case. However, as seen from Fig. 28(a), the tail of the Hushimi representation well overlaps with the classical separatrix. We can expect that an adiabatic transition occurs to an eigenstate with energy level around $E_n \simeq 0$ [50].

Under the stochastic perturbation with small perturbation strength, we observe that $H(t)$, $\Delta H(t)$, and $\Delta q(t)\Delta p(t)$ show oscillatory time dependence with recurrence to the initial values, as also observed in the polychromatic perturbation. However, in the time interval we simulated, the time dependence begins to show unbounded growth for the larger perturbation strength, different from the time dependence in the incoherent motion regime under the polychromatic perturbation.

APPENDIX C: FIDELITY

In this appendix we deal with fidelity $f(t)$ which is widely used to measure coherence of quantum dynamics [34,35]. We confirm consistency of the results between fidelity and degree of coherence defined by Eq. (15).

Fidelity $f(t)$ is defined by

$$f(t) = |\langle \psi(t=0)|U_0^\dagger U_\epsilon|\psi(t=0)\rangle|^2, \tag{C1}$$

where U_0 and U_ϵ denote the unperturbed and the perturbed time evolution operator, respectively.

Time dependence of $f(t)$ is shown in Fig. 29 for polychromatically and stochastically perturbed cases. In the former cases, a combination of the perturbation parameters corresponds to coherent, quasicoherent, or incoherent motion which are defined in Sec. IV.

When $M=1$ with several ϵ's shown in Fig. 29(a), each of which belongs to the coherent motion regime, $f(t)$'s oscillate with recurrence to the initial value. For small perturbation strength, $\epsilon=0.1$, fidelity satisfies $f(t)>0.9$. The amplitude of oscillation of $f(t)$ becomes larger with increase of the perturbation strength.

The time dependence of $f(t)$ when $M=3$ is given in Fig. 29(b). In the case of coherent motion ($\epsilon=0.1$), the behavior

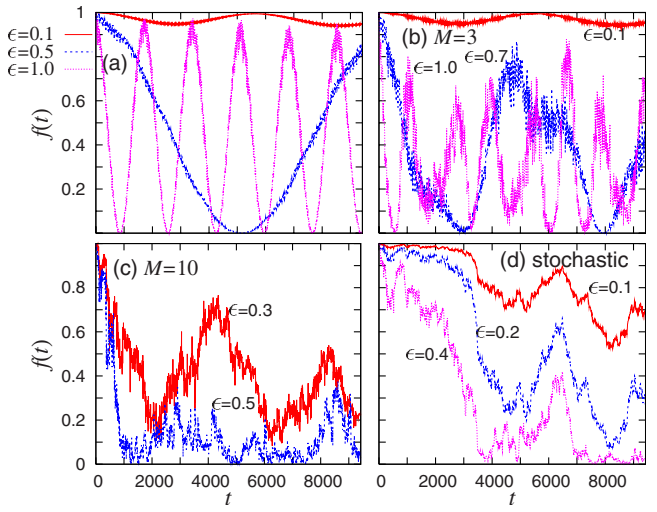

FIG. 29. (Color online) Time dependence of $f(t)$ for various combinations of the perturbation parameters. (a) The combination of the perturbation parameters are $M=1$ with $\epsilon=0.1$ (solid line), 0.5 (dashed line), and 1.0 (dotted line). (b) $M=3$ with $\epsilon=0.1$, 0.7, and 1.0. (c) $M=10$ with $\epsilon=0.3$ and 0.5. (d) Stochastically perturbed cases with $\epsilon=0.1$, 0.2, and 0.4.

is almost similar to that in the case $M=1$ with the same perturbation strength. On the other hand, in the cases of quasicoherent motion ($\epsilon=0.7$ and 1.0), $f(t)$'s show quite different time dependence from the weakly perturbed case. In the cases, $f(t)$ neither decays to zero nor return to the initial value. This is adequate to the property of a quasicoherent motion.

Time dependence of fidelity when $M=10$ is shown in Fig. 29(c). When the perturbation strength is relatively small, $\epsilon=0.3$, where quasicoherent motion occurs, we see similar time dependence to the cases $M=3$ with $\epsilon=0.5$ or $\epsilon=1.0$ in Fig. 29(b). On the contrary, in the case with $\epsilon=0.5$ corresponding to incoherent motion, $f(t)$ remains at the small value $f(t) \lesssim 0.3$ with irregular fluctuation after the rapid decrease.

Figure 29(d) shows time dependence of fidelity under the stochastic perturbation for several perturbation strengths. Recurrence of $f(t)$ to the initial value is not observed, although decay of $f(t)$ is not so rapid as seen in incoherent motion under the polychromatic perturbation.

As a result, time dependence of fidelity shows oscillation with recurrence to the initial value in the coherent motion regime. On the other hand, it fluctuates irregularly after the rapid decay in the incoherent motion regime. In the case of quasicoherent motion, it shows the intermediate behavior. In this sense, both the degree of coherence ΔP_L and fidelity $f(t)$ are effective as the measure of coherence in the quantum dynamics.

[1] W. A. Lin and L. E. Ballentine, Phys. Rev. Lett. **65**, 2927 (1990); Phys. Rev. A **45**, 3637 (1992).
[2] *Tunneling in Complex Systems*, edited by S. Tomsovic (World Scientific, Singapore, 1998).
[3] O. Bohigas, S. Tomsovic, and D. Ullmo, Phys. Rep. **223**, 43 (1993).
[4] A. Shudo and K. S. Ikeda, Physica D **115**, 234 (1998).
[5] L. Bonci, A. Farusi, P. Grigolini, and R. Roncaglia, Phys. Rev. E **58**, 5689 (1998).
[6] O. Brodier, P. Schlagheck, and D. Ullmo, Phys. Rev. Lett. **87**, 064101 (2001).
[7] D. A. Steck, W. H. Oskay, and M. G. Raizen, Science **293**, 274 (2001).
[8] I. Vorobeichik, E. Narevicius, G. Rosenblum, M. Orenstein, and N. Moiseyev, Phys. Rev. Lett. **90**, 176806 (2003).
[9] F. Grossmann, T. Dittrich, P. Jung, and P. Hänggi, Phys. Rev. Lett. **67**, 516 (1991).
[10] G. Della Valle, M. Ornigotti, E. Cianci, V. Foglietti, P. Laporta, and S. Longhi, Phys. Rev. Lett. **98**, 263601 (2007).
[11] D. L. Shepelyansky, Physica D **8**, 208 (1983).
[12] G. Casati, I. Guarneri, and D. L. Shepelyansky, Phys. Rev. Lett. **62**, 345 (1989).
[13] P. W. Milonni, J. R. Ackerhalt, and M. E. Goggin, Phys. Rev. A **35**, 1714 (1987).
[14] T. Dittrich and R. Graham, Ann. Phys. (N.Y.) **200**, 363 (1990).
[15] E. Ott, T. M. Antonsen, Jr., and J. D. Hanson, Phys. Rev. Lett. **53**, 2187 (1984).
[16] W. H. Oskay, D. A. Steck, and M. G. Raizen, Chaos, Solitons Fractals **16**, 409 (2003).
[17] L. Bonci, P. Grigolini, A. Laux, and R. Roncaglia, Phys. Rev. A **54**, 112 (1996).
[18] A. O. Caldeira and A. J. Legget, Ann. Phys. (N.Y.) **149**, 374 (1983); **153**, 445 (1984).
[19] W. H. Zurek, Rev. Mod. Phys. **75**, 715 (2003).
[20] S. Habib, K. Shizume, and W. H. Zurek, Phys. Rev. Lett. **80**, 4361 (1998).
[21] D. Cohen and T. Kottos, Phys. Rev. E **69**, 055201(R) (2004).
[22] Y. Yamaguchi, Phys. Lett. **109A**, 191 (1985).
[23] R. S. Zounes and R. H. Rand, Int. J. Non-Linear Mech. **37**, 43 (2002).
[24] M. Grifoni and P. Hänggi, Phys. Rep. **304**, 229 (1998).
[25] A. Igarashi and H. Yamada, Chem. Phys. **309**, 95 (2005).
[26] A. Igarashi and H. Yamada, Physica D **221**, 146 (2006).
[27] M. Thorwart, P. Reimann, P. Jung, and R. F. Fox, Chem. Phys. **235**, 61 (1998).
[28] A. J. Lichtenberg and M. A. Lieberman, *Regular and Chaotic Dynamics* (Springer-Verlag, Berlin, 1990).
[29] B. V. Chirikov, Phys. Rep. **52**, 263 (1979).
[30] M. Razavy, *Quantum Theory of Tunneling* (World Scientific, Singapore, 2003).
[31] K. Takahashi and K. Ikeda, J. Chem. Phys. **99**, 8680 (1993).
[32] L. Baroni, A. Cuccoli, V. Tognetti, and R. Vaia, Physica D **113**, 374 (1998).
[33] J. Plata and J. M. Gomez Llorente, J. Phys. A **25**, L303 (1992).
[34] A. Peres, Phys. Rev. A **30**, 1610 (1984).
[35] T. Prosen, Phys. Rev. E **65**, 036208 (2002).
[36] L. Bonci, R. Roncaglia, B. J. West, and P. Grigolini, Phys. Rev. A **45**, 8490 (1992); **46**, 8034(E) (1992).
[37] E. J. Heller, in *Chaos and Quantum Physics*, edited by M. -J. Giannoni, A. Voros, and J. Zinn-Jusitin (North Holland, Amsterdam, 1991).
[38] K. Takahashi, Prog. Theor. Phys. Suppl. **98**, 109 (1989).
[39] B. S. Helmkamp and D. A. Browne, Phys. Rev. E **49**, 1831 (1994).
[40] M. V. Berry, N. L. Balazs, M. Tabor, and A. Voros, Ann. Phys. (N.Y.) **112**, 26 (1979).
[41] S. Habib, K. Jacobs, H. Mabuchi, R. Ryne, K. Shizume, and B. Sundaram, Phys. Rev. Lett. **88**, 040402 (2002).
[42] G. M. Zaslavsky, Chaos **1**, 1 (1991).
[43] W. Zhu, J. Botina, and H. Rabitz, J. Chem. Phys. **108**, 1953 (1998).
[44] S. A. Rice and M. Zhao, *Optimal Control of Molecular Dynamics* (Wiley, New York, 2000).
[45] N. Došlić, O. Kün, J. Manz, and K. Sundermann, J. Phys. Chem. A **102**, 9645 (1998).
[46] M. Artamonov, T-S. Ho, and H. Rabitz, J. Chem. Phys. **124**, 064306 (2006).
[47] A. R. Kolovsky, Chaos **6**, 534 (1996).
[48] A. Bassi and G. C. Ghirardi, Phys. Rev. A **65**, 042114 (2002).
[49] A. M. Jayannavar and N. Kumar, Phys. Rev. Lett. **48**, 553 (1982).
[50] R. Utermann, T. Dittrich, and P. Hänggi, Phys. Rev. E **49**, 273 (1994).